Building a 3D Seismic Velocity Model to Improve Location of Microseismic Events at the Åknes Rock Slope

Helge Wilhelm Dahl

Master's thesis in Geoscience
Geophysics Program
60 credits

Department of Geosciences
Faculty of Mathematics and Natural Science
UNIVERSITY OF OSLO
Norway
Spring 2020

Building a 3D Seismic Velocity Model to Improve Location of Microseismic Events at the Åknes Rock Slope

by
Helge Wilhelm Dahl

Building a 3D Seismic Velocity Model to Improve Location of Microseismic Events at the Åknes Rock Slope

Supervisors: Volker Oye, Nadege Langet and Valerie Maupin

http://www.duo.uio.no/

Abstract

The Åknes rock slope is a geohazardous area in western Norway where an unstable rock slope, covering an area of approximately $1km^2$, is slowly sliding towards the fjord. If a sudden failure were to occur, the rock mass hitting the fjord would generate a tsunami, causing destruction to the nearby localities.

The upper part of the slope is affected by the largest extensional forces, and explains why a permanent seismic network was installed here. It consists of 8 geophones continuously gathering seismic data. Our study area in this project is constrained by the network's location.

The goal of the network is to detect, locate and classify seismic events. Successfully locating events is difficult, as the precision of the locations is reduced by the limited knowledge on the seismic velocity structure. In this project we improve this knowledge by building a seismic velocity model able to explain the P-wave arrival times recorded by the geophones. The data used to develop the model were generated by shots (small explosions) from a controlled seismic experiment with known locations and timings.

The velocity structure was gradually made more complex from homogeneous to heterogeneous in several steps. Firstly the surface layer was modeled using the shot data. Secondly the model was expanded by increasing the velocities with depth. Finally, assumed geological features were added: A high velocity zone defined by a sliding plane at a depth of $50m$ and a low velocity zone surrounding a graben structure.

The model containing all of these features shows great improvement compared to the homogeneous velocity models. It was used to locate naturally occurring seismic events with presumed locations. The events were located close to their expected positions, which indicates that the model is a good representation for the velocities in the area.

The final 3D seismic velocity model will be used by NORSAR to locate the events in near-real time, which could help improve their warning system for the area.

Acknowledgements

Several people have helped me along the way, this past year, when working on this master thesis. My supervisors, Volker, Nadege and Valerie, made the project possible, and were all very helpful. Discussing our projects and drinking coffee with my fellow master students, Marcus, Mathilde and Trine, has also been a great help (pre-pandemic). We kept in touch while we were all stuck at home, through a group chat or having a beer over a video call. Marcus deserves an extra credit, as he helped me out with some of the more frustrating parts of the programming process. I would also like to thank my girlfriend, sister and father, for discussing the project and pitching ideas. My mother read the project, and helped me keep my motivation. Lastly I would like to thank Hamza for reading the thesis and providing some last-minute feedback.

Contents

List of Figures

List of Tables

1 Introduction

Figure 1: Map showing the location of the Åknes site (from Google maps).

Åknes is located in Møre og Romsdal in the western part of Norway. The Åknes rock slope is an unstable part of the mountain, situated on the western flank of the fjord Sunnylvsfjorden, a branch of the larger Storfjorden (Figure 1). The three localities Stranda, Geiranger and Hellesylt are located in Sunnylvsfjorden, some kilometers away from the rock slope. The respective populations of the localities are approximately 4600, 4500 and 260. The fjord Geirangerfjorden, which is one of Norway's most visited tourist attractions, is a branch of Sunnylvsfjorden. It is registered on UNESCO's world heritage list. Up to 200 cruise ships and 700,000 tourists visit the area every year. If a collapse of the unstable rock-slope were to occur, large rockmasses would fall into the fjord, creating a tsunami (Fischer et al., 2019). This makes Åknes a potential geohazard for the nearby localities, which inspired the Norwegian disaster-movie 'The Wave' from 2015.

The goal of this project is to improve the location of microseismic events in the upper part of the unstable Åknes rock slope. Due to the heavily fractured medium dominating the area, locations based on homogeneous seismic velocity models give unsatisfactory results. A more complex, heterogeneous 3D seismic velocity model is needed. The data set used in this project is from a seismic experiment from 2006, where 11 calibration shots and a network of 8 permanent geophones were used. In this case the known position of the shots and geophones, together with interpreted traveltimes, were used to produce a

velocity model (NORSAR, 2006). Automatic seismic tomography is often used to create velocity models in cases like this. However, the data set used in this project is very limited, and it is not feasible to conduct a reliable, automatic tomography. Therefore we used a manual approach instead, to get a better idea of the velocity model. This was combined with manually implementing assumed and suggested geological features present at the slope. An automated tomography is limited by the nature of the shots. It would not get a unique solution for the deeper geological features, because of the limited date coverage. This makes a manual approach even more preferable.

The new and improved seismic velocity model will give a better understanding of the varying velocities in the area. It can, ultimately, be used to locate natural events. This will be helpful when monitoring the movement of the unstable Åknes rock slope, which can improve the existing real-time warning system for mitigation in this geohazardous area.

2 Åknes

2.1 The Åknes rock slope - a potential geohazard

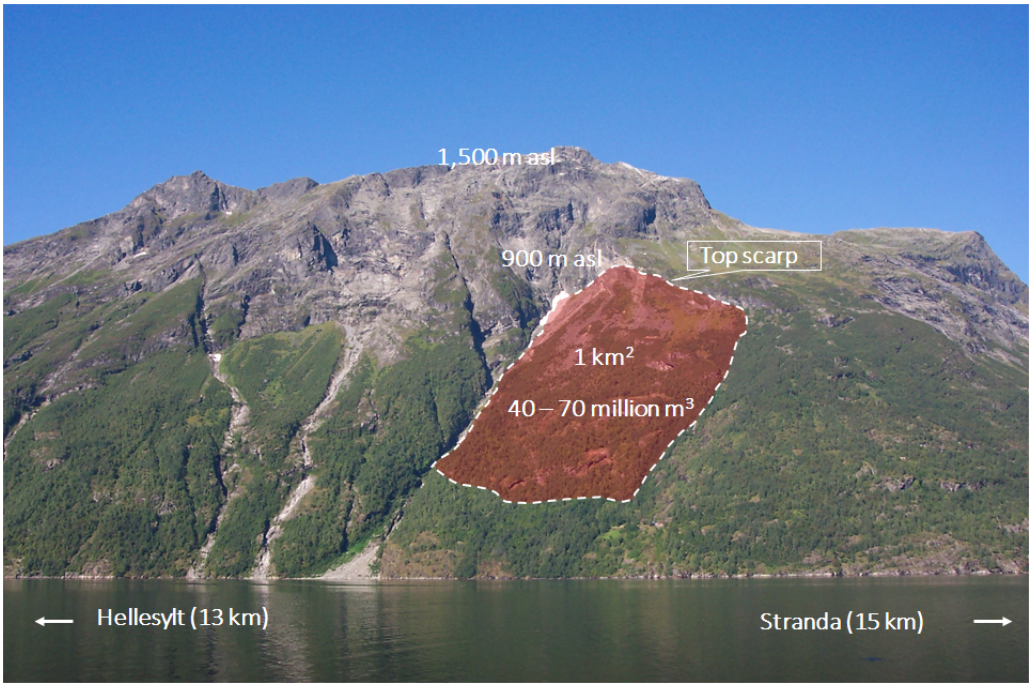

Figure 2: The unstable Åknes rock slope is marked in red (Roth et al., 2006).

The Åknes geological site is located in the western part of Norway. It mostly consists of quartzo-feldsparic gneisses. The unstable part of the rock slope covers an area of approximately 1 km^2 (Roth et al., 2006) (Figure 2). A sliding plane separates the rock slope from the stable part of the mountain. The location of this sliding plane is still not precisely determined, making the depth and total mass of the unstable area uncertain.

Various articles suggest different depths for the sliding plane. Blikra et al. (2013) suggests a depth of $50m$, based on the Differential Monitoring of Stability (DMS) method, where the displacement in depth is measured. Kveldsvik (2008) suggests a depth of $120m$, based on measurements from a borehole in the upper part of the slope. Nordvik et al. (2009) suggests several different scenarios with undulating sliding planes: $40 - 55m$, $105 - 115m$ and $150 - 190m$. The total mass has been estimated to be within the range of 40 to

70 million m^3 (Roth et al., 2006). However, it is important to note that all estimations are uncertain. The rates of displacement are largest in the upper part, measured to be $14cm/year$. In the lower part there is an upwards displacement of 1 to $3cm/year$, due to compression (Fischer et al., 2019). The upper part of the deformed area is defined by a graben structure, which is reduced to a crack towards the south east. This is a result of the extensional fractures caused by the downward movement of the slope (Braathen et al., 2004).

Due to an increased population in the nearby localities and an increase in tourism in the Norwegian fjords, a failure of the rock slope leading to a tsunami could be disastrous. Although the total mass of the potential geohazardous area is unknown, several tsunami scenarios have been modelled and tested in lab experiments. A worst case scenario model run by Harbitz et al. (2014) resulted in an $85m$ high tsunami reaching Hellesylt, and a $70m$ high tsunami reaching Geiranger. These numbers are based on a rockslide with a volume of more than 50 million m^3.

Rockslides and related tsunamis are constant dangers in the western part of Norway, even though they happen rarely. They are among the geohazards with the largest capacity of destruction in the country. In the past 100 years, more than 170 people have lost their lives to this type of disasters. With modern methods, the geohazards can be monitored, and the loss of lives can be prevented. Looking back at the geological history of Norway, one can find several occurrences similar to what could happen at the Åknes rock slope. It is safe to assume that a disastrous event at Åknes is a dangerous and likely scenario at some point in the future (Blikra et al., 2006).

2.2 The geophone network

A permanent seismic network was installed in November 2005, measuring the seismic activity on the Åknes rock slope. It is located in the upper part of the slope, and consists of 8 3-component geophones, covering a 250 by $100m$ area at an altitude from 762 to $862m$ above sea level (Figure 3). Each geophone is connected to a central acquisition

system by an armoured cable with lightning protection. The geophones do not need a power supply as they are passive sensors. The incoming seismic data are temporarily stored in the central system, before being transferred to NORSAR for permanent storage and processing (Langet, 2018). A file is only created and sent to NORSAR if there are simultaneous detections at several geophones, meaning that they receive only triggered and not continuous data.

Although the geophones are protected, some of them have been damaged during the years. The cables connecting the geophones to the central acquisition system are the weak points of the network, and can easily be damaged or destroyed by rockfalls and snow avalanches. Therefore the data availability has varied over the years, and there are some inconsistencies in the data. However, annual repairs of the cables are usually conducted. Currently, 3 of the 8 geophones are out of order, due to cut cables (Langet, 2018). Still, there are several years of good data, with tens to hundreds of registered events each day (Fischer et al., 2019).

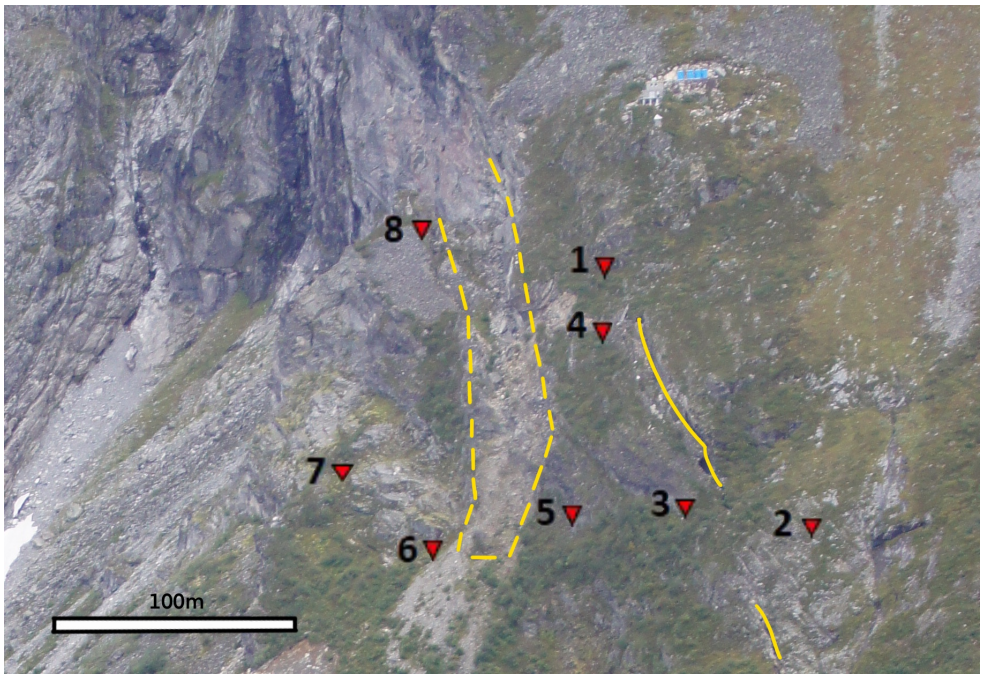

Figure 3: Photo from the upper part of the slope showing the geophone network, where each geophone's approximate position is marked with a red triangle. The geophone network is approximately 250x100x110m. The position of a graben structure is approximately marked by the yellow stippled line, and visible parts of a larger crack are marked by the yellow lines. Photo by Nadege Langet.

2.3 Data

The data used in this project are mostly from 11 calibration shots done during an experiment at the Åknes rock slope in 2006. 11 shot positions were selected, within and around the area bordered by the geophone network. The shot positions are presented in table 1. To execute the shots, shallow boreholes were drilled into solid rock or large blocks and explosives were inserted and detonated separately. The data collected from this experiment, consist of the traces of all shots recorded by all geophones (NORSAR, 2006). This resulted in 88 traces, each having a north, east and vertical component (Figure 4). The plots show the waveforms of the data, where a first arriving pressure-wave (P-wave) and a strong sound-wave can be observed. The horizontal axis starts at 2000ms, as the data have a added delay before the shots were fired. The straight blue line, represents the sound-wave velocity of 330m/s, which more or less lines up with the sound waves in

the traces. The other straight lines represent homogeneous velocities. The first arriving P-waves do not line up with any of these lines, which shows that the area cannot be represented by one specific velocity. It might also indicate that the waves follow different ray-paths.

	Northing (UTM) $[m]$	Easting (UTM) $[m]$	Depth (- altitude) $[m]$
Shot 1	6896082	395415	-852
Shot 2	6896070	395381	-861
Shot 3	6896019	395370	-839
Shot 4	6895999	395310	-848
Shot 5	6895993	395272	-859
Shot 6	6896042	395268	-872
Shot 7	6895971	395299	-820
Shot 8	6895944	395361	-772
Shot 9	6895950	395344	-789
Shot 10	6895953	395430	-744
Shot 11	6895966	395471	-745

Table 1: The true locations of the 11 calibration shots from 2006. MStudio operates with a z-axis with positive numbers in depth, making the positions above sea level negative.

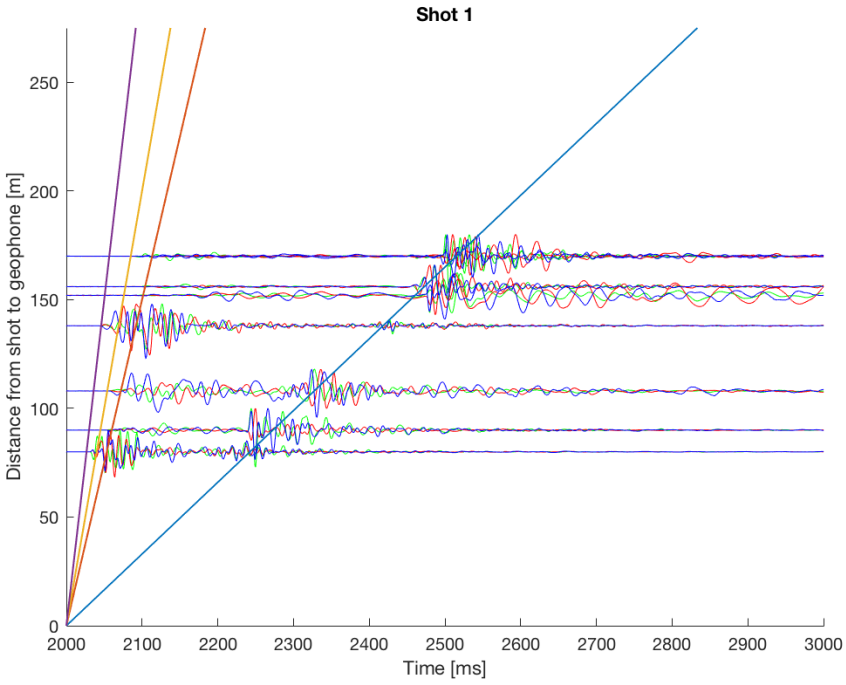
Shot 1
Distance from shot to geophone [m]
Time [ms]
0
50
100
150
200
250
2000
2100
2200
2300
2400
2500
2600
2700
2800
2900
3000

(a)

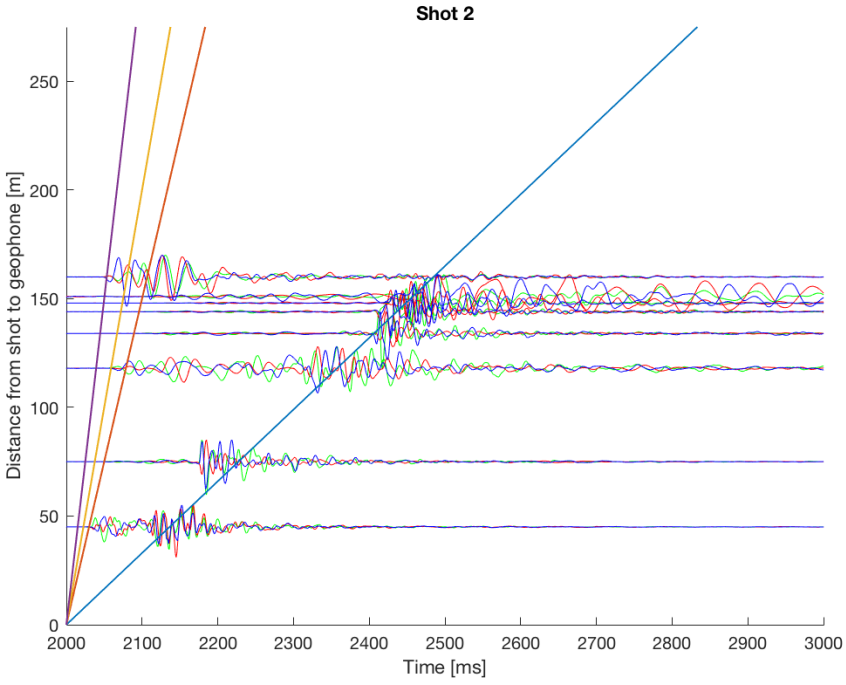
Shot 2
Distance from shot to geophone [m]
Time [ms]
0
50
100
150
200
250
2000
2100
2200
2300
2400
2500
2600
2700
2800
2900
3000

(b)

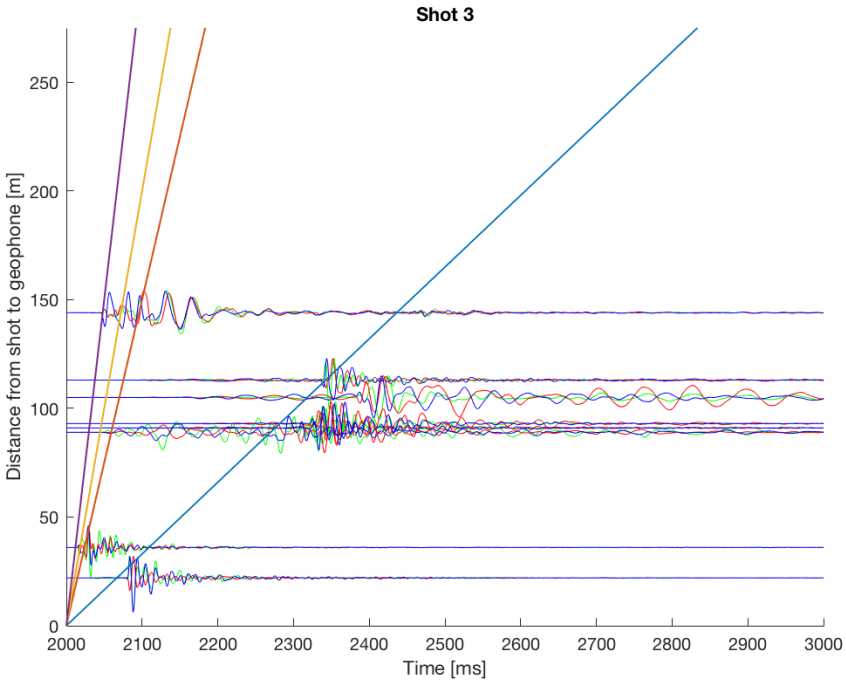
Shot 3
Distance from shot to geophone [m]
Time [ms]
0
50
100
150
200
250
2000
2100
2200
2300
2400
2500
2600
2700
2800
2900
3000

(c)

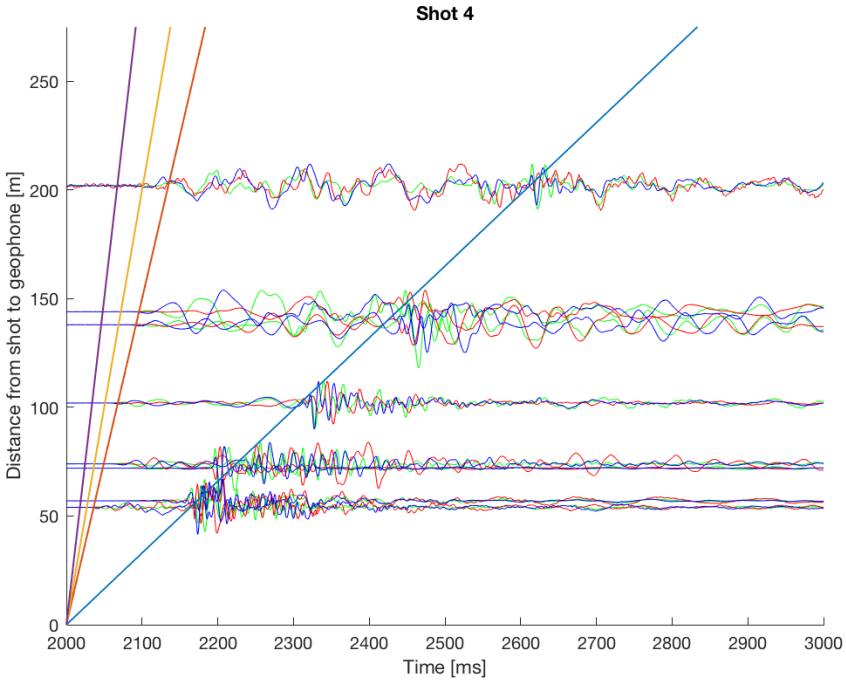
Shot 4
Distance from shot to geophone [m]
Time [ms]
0
50
100
150
200
250
2000
2100
2200
2300
2400
2500
2600
2700
2800
2900
3000

(d)

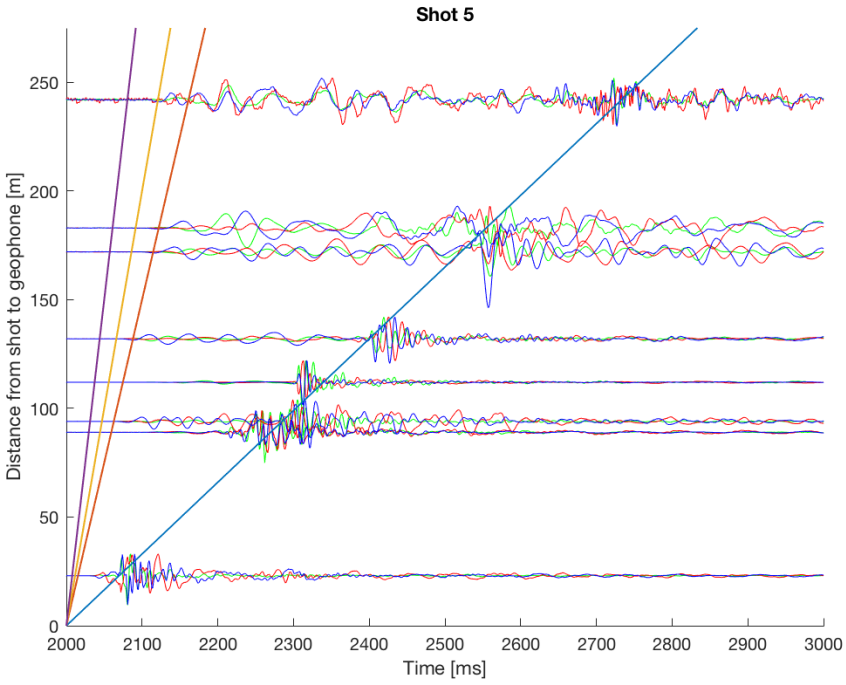
Shot 5
Distance from shot to geophone [m]
Time [ms]
0
50
100
150
200
250
2000
2100
2200
2300
2400
2500
2600
2700
2800
2900
3000

(e)

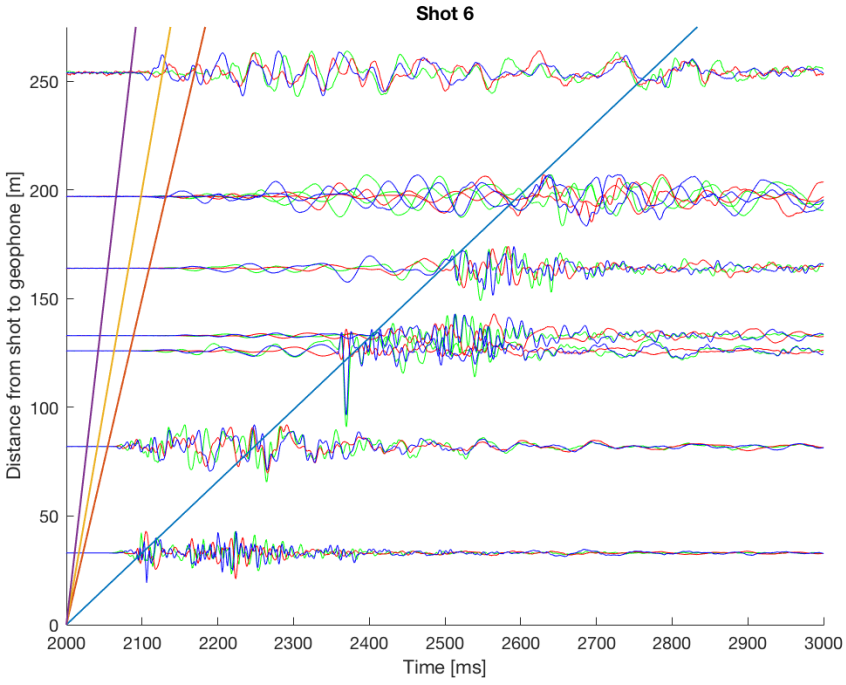
Shot 6
Distance from shot to geophone [m]
Time [ms]
0
50
100
150
200
250
2000
2100
2200
2300
2400
2500
2600
2700
2800
2900
3000

(f)

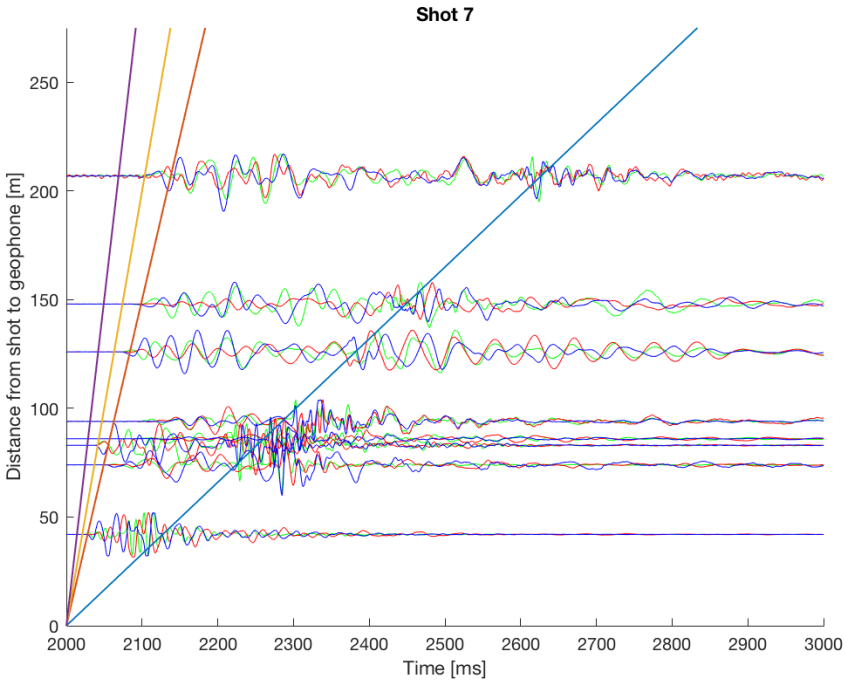
Shot 7
Distance from shot to geophone [m]
Time [ms]
0
50
100
150
200
250
2000
2100
2200
2300
2400
2500
2600
2700
2800
2900
3000

(g)

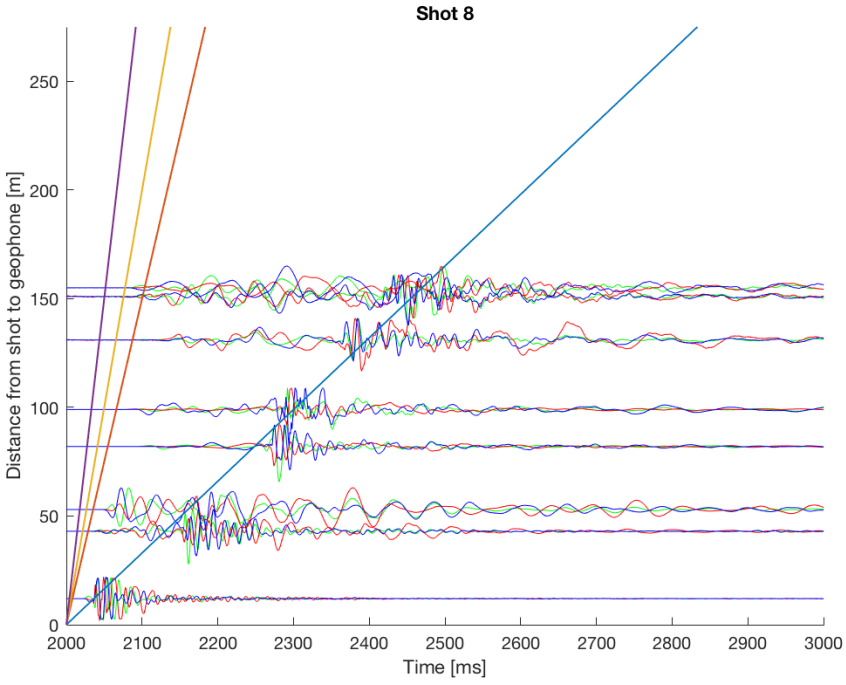
Shot 8
Distance from shot to geophone [m]
Time [ms]
0
50
100
150
200
250
2000
2100
2200
2300
2400
2500
2600
2700
2800
2900
3000

(h)

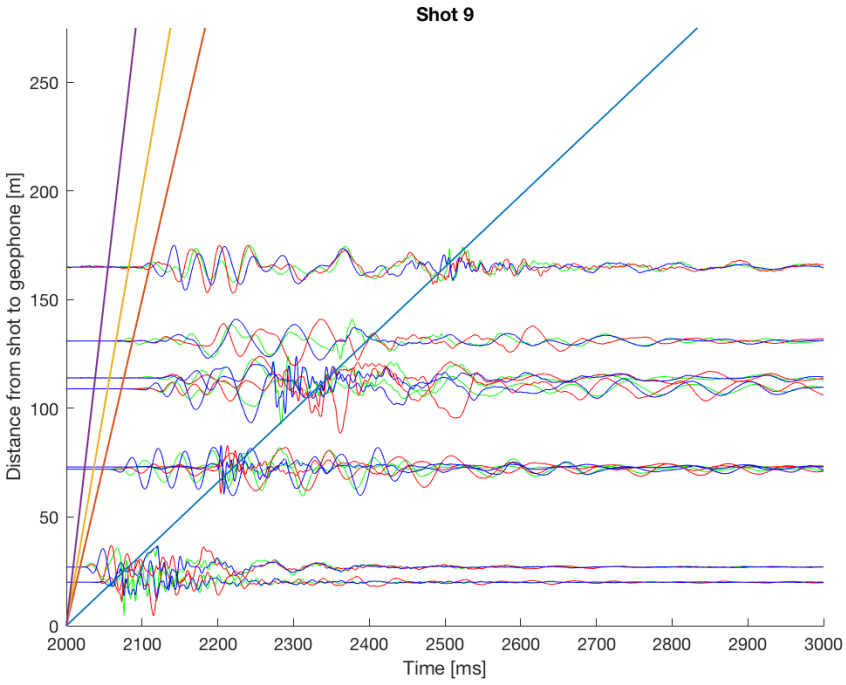
Shot 9
Distance from shot to geophone [m]
Time [ms]
0
50
100
150
200
250
2000
2100
2200
2300
2400
2500
2600
2700
2800
2900
3000

(i)

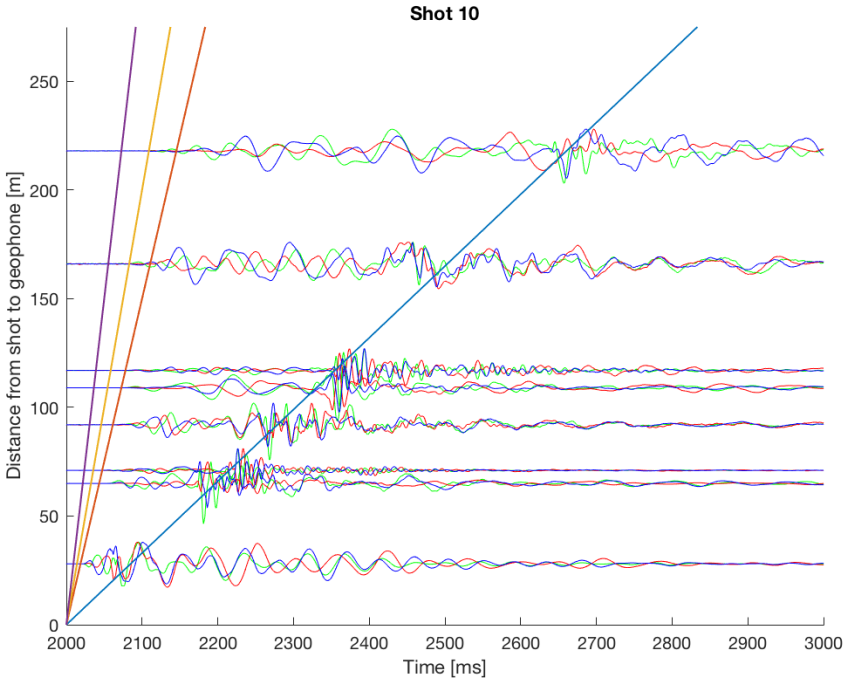
Shot 10
Distance from shot to geophone [m]
Time [ms]
0
50
100
150
200
250
2000
2100
2200
2300
2400
2500
2600
2700
2800
2900
3000

(j)

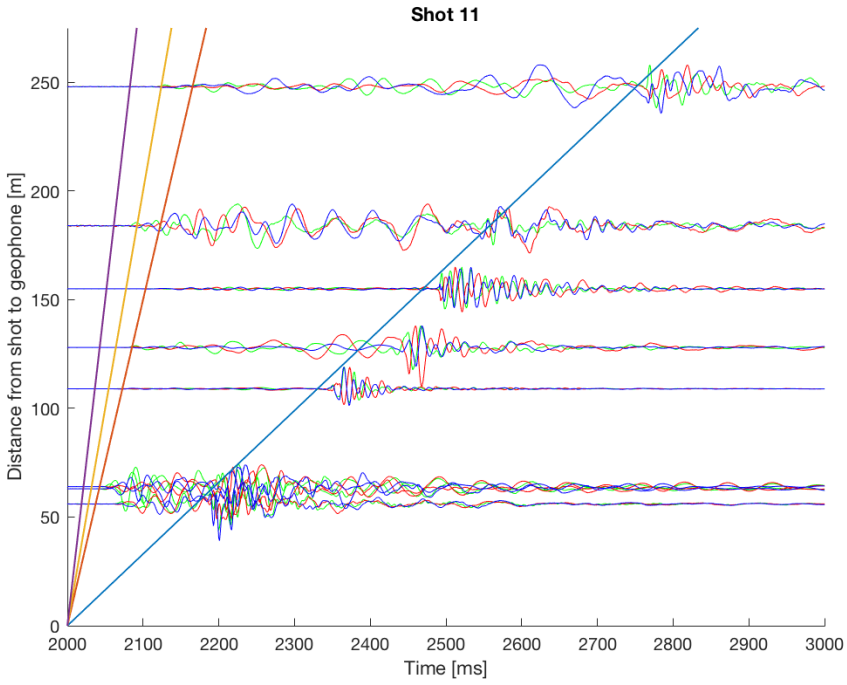

(k)

Figure 4: The plots above show shots 1 to 11 recorded by the 3-component geophones. North, east and depth are represented by red, blue and green traces respectively. The traces are arranged by the distance between each shot and geophone. The four straight lines represent homogeneous velocities, where the purple line is 3000 m/s, the yellow is 2000 m/s, the red is 1500 m/s and the blue line represents the sound wave velocity of 330 m/s.

The ultimate goal of this project is to create an accurate seismic velocity model, which can be used to locate naturally occurring events. The work in this thesis has attempted to locate several such events, recorded by the geophone network. Figure 5 shows two examples of data form local events. There can be a big difference between the data resulting from controlled experiments and naturally occurring events. The former often result in cleaner plots, with a higher signal-to-noise ratio. The latter are often of poorer quality, with more noise. The quality can also vary between different naturally occurring events. This is mainly due to different amounts of energy and varying noise conditions. Event (a) is probably larger than event (b), making it more dominant compared to the noise. It is also important to note that some geophones might be out of order at the time of

recording, which is the case for the example events (Figure 5). Geophones 6, 7, and 8 were out of order in case (a). The event in case (b) is more complicated. In this case geophones 3 and 4 registered the event clearly, but only geophones 5 and 7 were out of order. The remaining geophones registered a lot of noise in the data, and it is difficult to pick out the event.

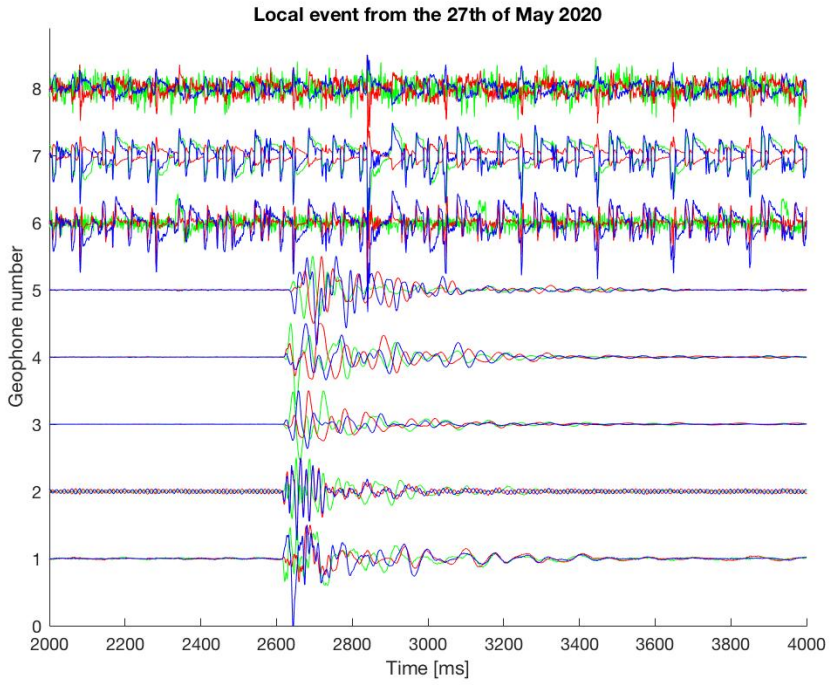

(a)

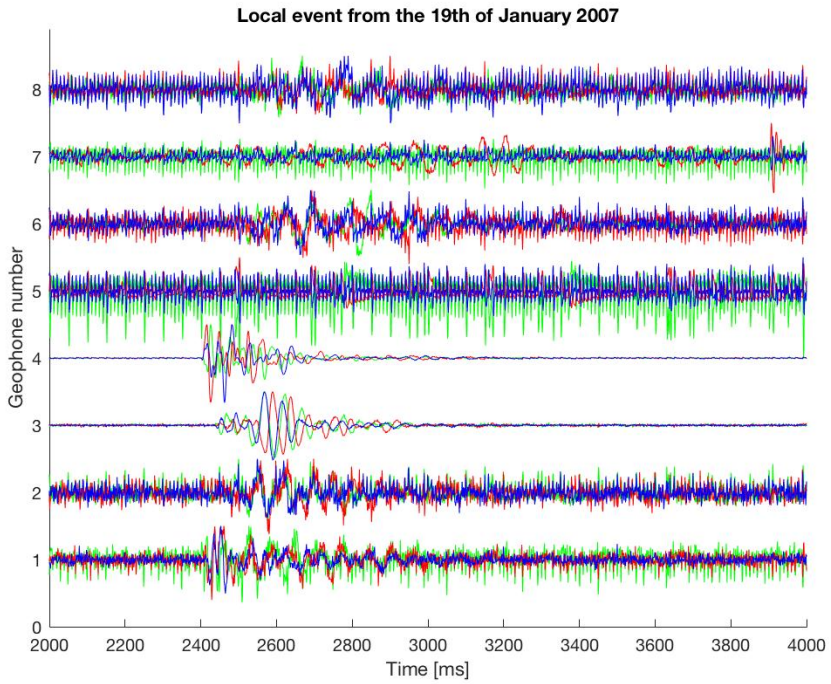

(b)

Figure 5: Example data from two local events form 2007 and 2020.

2.4 Study area

The study area for this project is centered around the 8 geophones and 11 calibration shots from 2006. It is located at UTM coordinates 395150 to 395550 $[m]$ in the east-west axis, and UTM 6895900 to 6896100 $[m]$ in the north-south axis. The altitude is from 700 to 900 meters above sea level. The study area is defined as a rectangular prism, with dimensions of 400x200x200m (Figure 6). It stretches farther in the west than the east direction to include the graben structure, located close by geophone 8, which is a product of the heavy extensional deformation (Braathen et al., 2004). All upcoming velocity models have the same measurements, which means that they cover the same area.

We have chosen this area because the geophone network is located here, providing enough data to make the project doable. This is also where an improved velocity model is needed. The accurate velocities in this area are unknown, and assumed to vary rapidly. Therefore the usage of a homogeneous velocity model does not work well. We do have an applicable velocity model for the lower parts of the Åknes rock slope, derived form refraction seismic experiments in 2004 and 2005. The result was a three-layered 1D velocity model for this area (NORSAR, 2006). However, since the velocities are different in the different parts of the slope, this model cannot be applied to our chosen study area.

The coordinate system for this project is the same for the study area and all upcoming velocity models. It is defined by the vertical and horizontal planes. The x-axis is aligned with the eastern direction, the y-axis is aligned with the northern direction and the z-axis is aligned with the altitude/depth. The size of the geophone network, study area and upcoming velocity models are shown in table 2. The resolution used throughout the project is 5x5x5m.

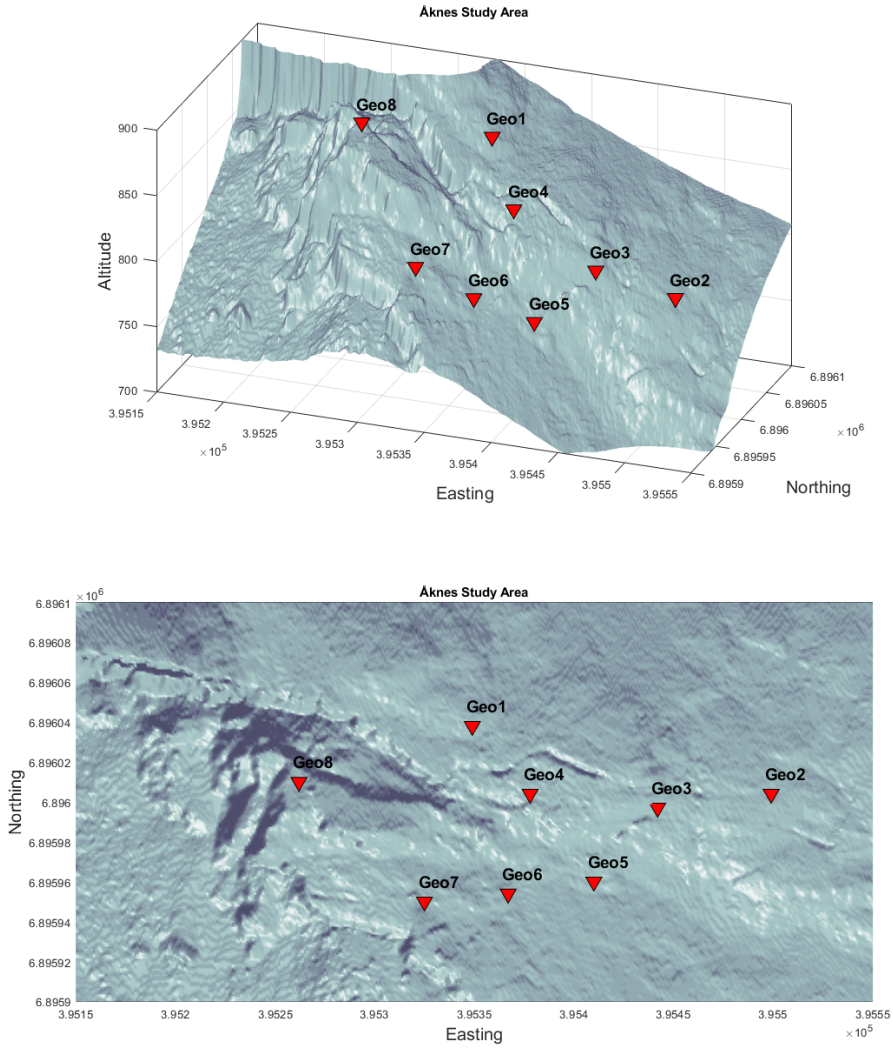

Figure 6: A 3D model of the study area at the upper part of the unstable Åknes rock slope, shown from two different angles. The geophones are marked in red triangles. The axes show UTM coordinates $[m]$ and the total size of the study area is 400x200x200m

Size of geophone network	250x100x110 $[m]$
Size of study area	400x200x200 $[m]$
Size of 3D models	400x200x200 $[m]$
Size of grid-cells/resolution	5x5x5 $[m]$

Table 2: The sizes of the geophone network, study area, 3D velocity models and grid-cells/resolution.

2.5 Seismic event location

To locate an event, we need a velocity model for the area and a minimum number of observations across the network. The velocity model gives the theoretical traveltimes. The most common way of locating an event is to pick the P- and/or shear-wave (S-wave) arrival times. They are picked and measured at the individual geophones as the waves pass through. The arrival times are then inverted to locate the events (Retailleau et al., 2015).

This project uses a full grid-search location algorithm to obtain locations. Simpler and quicker algorithms exist, but they are less accurate. In this project we have a limited data set and therefore time and resources to use an algorithm that requires longer computational time. Different velocity models, both homogeneous and heterogeneous, have been inserted into the full grid-search location algorithm, to derive locations of increasing accuracy. The algorithm calculates the residuals (the time difference between observed and theoretical picks) and combines them into a single value with a least square misfit function. This is done in each grid-cell, which is colour coded according to the function. The location is placed where the misfit is at its minimum.

To locate larger events one can look at the time difference between P- and S-waves as they arrive at different stations. However, this only works when there are clear onsets of both P- and S-waves and a large enough time difference between them, making them distinguishable. This method does not work in our project, since the data set consists of small-size events. This gives only one readable peak, the first arriving P-wave, and

therefore only one arrival time to be used in the locations.

Fischer et al. (2019) locates calibration shots on the Åknes rock slope, using the same data set as this project. However, our methods differ. Instead of using the picked arrival times, they locate events using the migration stacking method. This method uses the energy of the arriving seismic waves instead of the arrival times. Also, they only use homogeneous velocity models, while we use both homogeneous and heterogeneous models. Using a homogeneous velocity model with $V_p = 1500m/s$ produced their best results. The authors state that standard methods of arrival picking do not work, as S-waves are not present in the data.

2.5.1 Creating velocity models

Automatic seismic tomography is often used to model the velocities in the subsurface. In other words, constructing a velocity model. It uses the seismic waves from explosions or earthquakes. The data obtained, can then be used to solve an inverse problem. A solution will derive 3D images of velocity anomalies in the area. It can be non-unique, depending on the amount of data used. This means there can be several velocity models that all fit the data equally well. More data from shots, explosions or earthquakes will give a more detailed data set with fewer possible velocity models. With a larger data set, seismic tomography is one of the best ways to create a complex velocity model of an area.

An automatic seismic tomography is not used in this project. We think that it would yield a less accurate result than our method, due to a very limited data set. After all, we only have data form 11 surface shots to create the velocity models. Additional shots to get a denser coverage of the area would probably make it possible to derive an accurate velocity model from an automatic seismic tomography (NORSAR, 2006). It is important to note that our method is based on minimizing an error function, similar to the automated tomography. In addition, we manually implemented the assumed geological features into the velocity model in MatLab. This was done by trial and error, checking the results for each added feature. A feature was kept if the results improved and discarded if they declined.

3 Method

3.1 MStudio

The main program used in this project is MStudio (Figure 7), a seismic processing program provided by NORSAR. It is written in MatLab, and has many applications within the seismic processing field. The program works by importing, organizing and processing seismic data. By opening the data in a tab called 'Wavelab' (Figure 8), individual traces can be viewed and processed. Here, the data can be quickly filtered and scaled to make them easier to interpret.

This is also where the first arriving P- and S-waves (or sound-waves) can be picked automatically or manually along the time-axis, if they are available in the data set. Manually picking the first arrivals gives more control of the data, as opposed to automatic picks where the accuracy of the picks is unknown. One needs to choose how the event picks should be performed. In this project the picks were done manually, as the amount of available data were manageable. The waves are picked when they reach the geophones, and the arrival-times are saved. This is the first step in the process of locating seismic events.

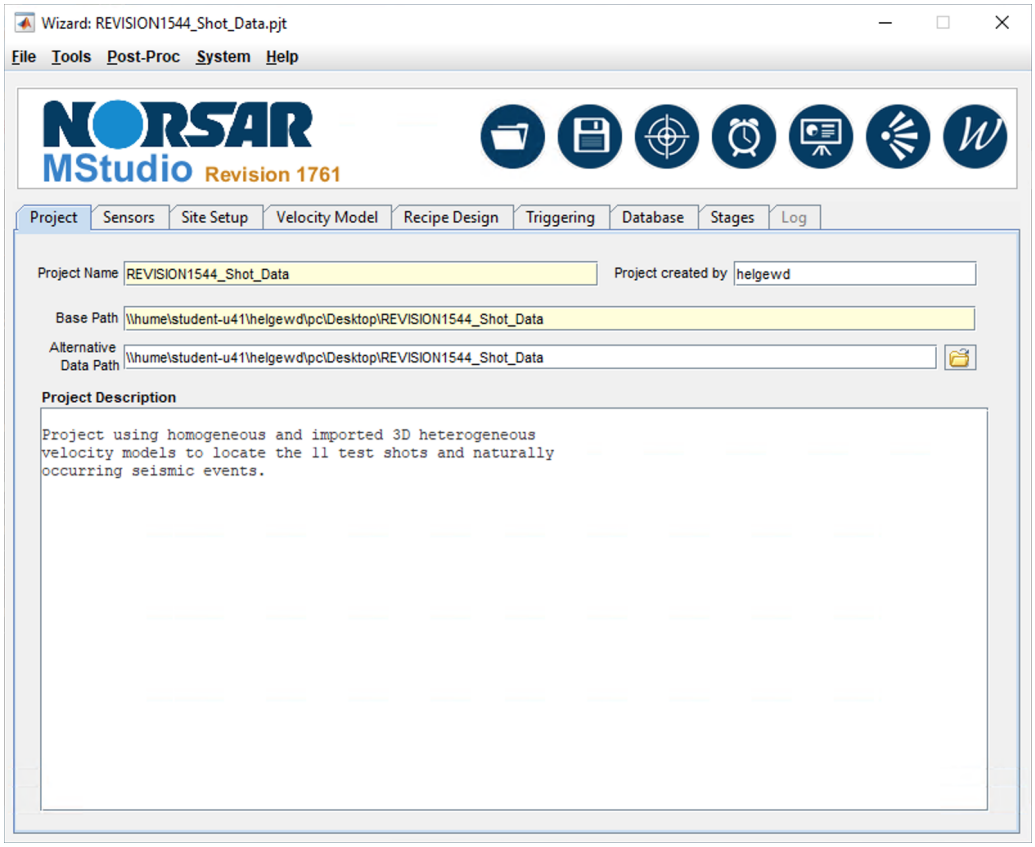

Figure 7: The MStudio Wizard is the menu for the program. Here one can select different tabs and tools for viewing and processing seismic data.

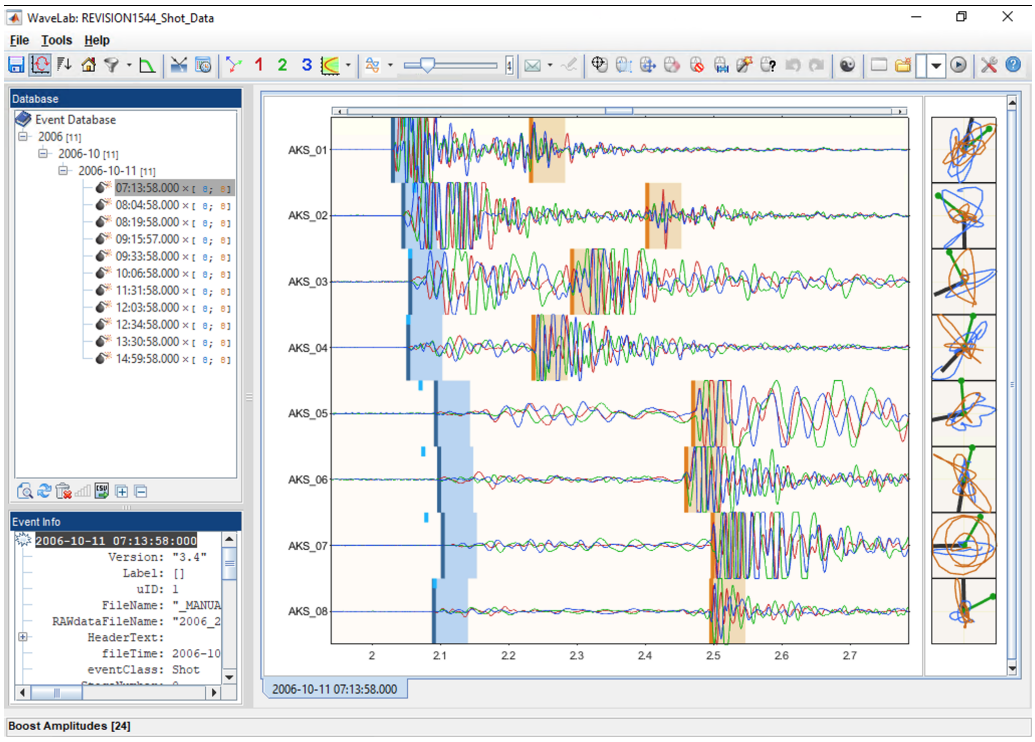

Figure 8: Data from calibration shot 1, viewed in MStudio. It shows the traces registered by each geophone. The vertical blue lines are the manually picked first arriving P-waves and the vertical orange lines are the manually picked sound-waves.

In this project, the data from the 11 calibration shots are of high quality and have a high signal-to-noise ratio. The only required pre-processing needed on the data are seismic-wave picks.

The most important tool in MStudio for this project are sequences of relevant processing that can be applied to the data. These include filtering, automatic event picking or event location, using different location algorithms. These sequences are called recipes in MStudio. They make it possible to execute the exact same processes to different data, or data sets. In the case of this project, the location recipes use the full grid-search location algorithm.

Homogeneous velocity models and 1D velocity models (which we did not use) can be made directly in MStudio (figure 9). Homogeneous velocity models are created by having the

same velocity at all depths. More complex heterogeneous models with velocity changes in more than one direction, must be made outside of MStudio and imported into the program to be used in the location recipes.

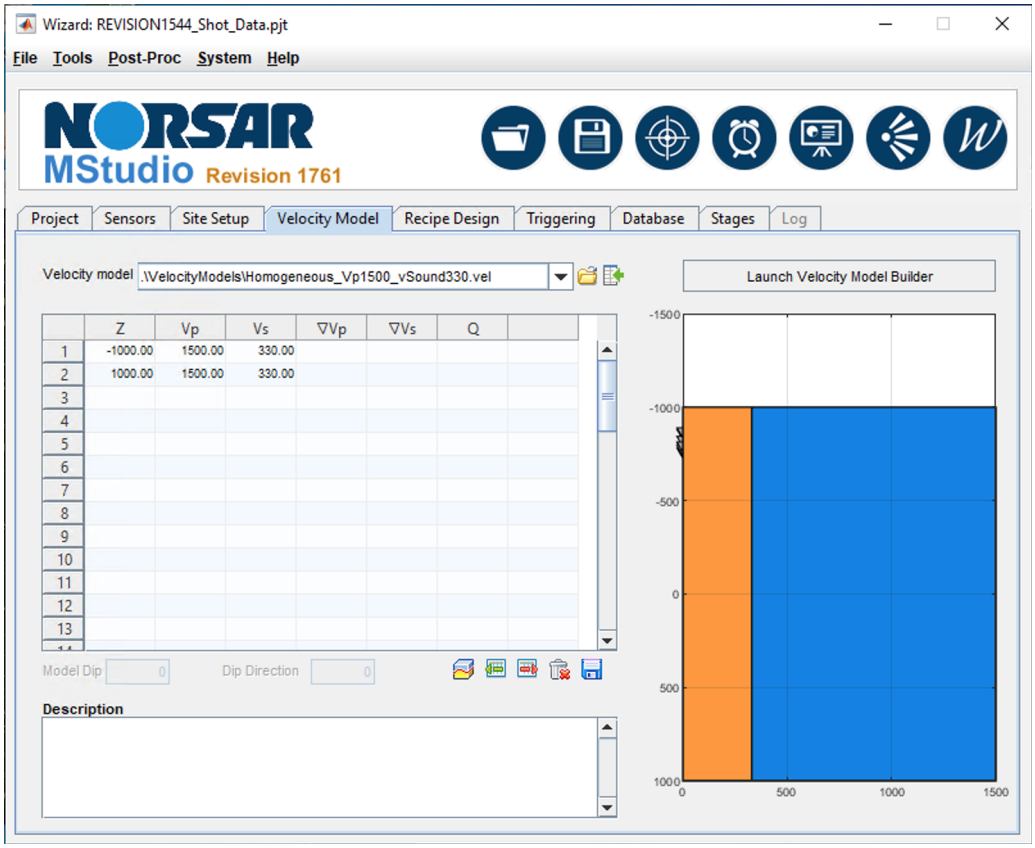

Figure 9: MStudio's 1D velocity model builder, with an example of a homogeneous velocity model with a P-wave velocity of $1500m/s$ (blue) and a sound-wave velocity of $330m/s$ (orange).

Each velocity model was used to derive 8 theoretical traveltime tables, one for each of the 8 geophones. The traveltime tables are computed in MStudio. In the program the Eikonal equation, which describes the movement of the wavefront, is solved via the finite difference method using the fast-marching algorithm. The traveltime tables are centered around the geophones instead of the shots, because the locations of the geophones have constant positions. In a homogeneous case, the wavefront moves out from the event focus as a perfect sphere (Figure 10). In a heterogeneous case the wavefront will move at

different velocities in different directions, and the the traveltime table will not be spherical.

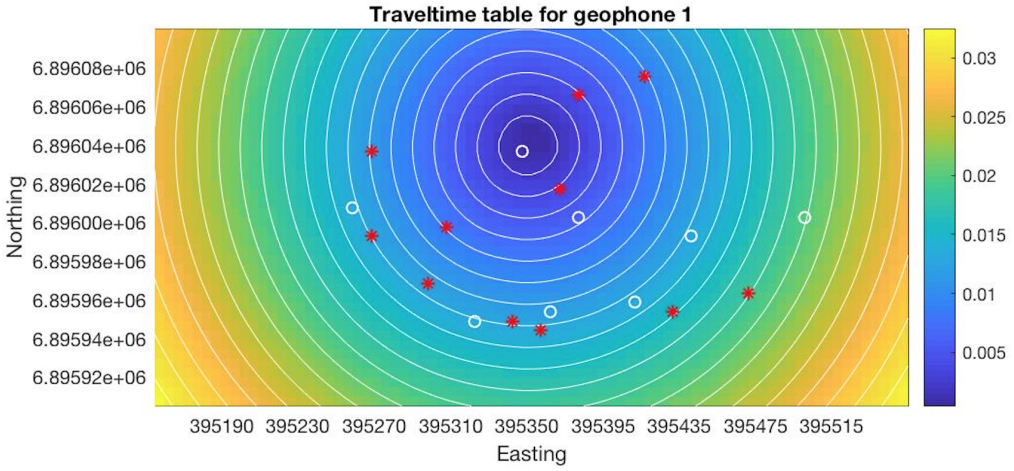

Figure 10: The traveltime table centered around geophone 1, derived from the velocity model with a P-wave velocity of $1500m/s$. The colour bar shows the traveltimes $[s]$. The figure was created using a script by Raanes (2011).

MStudio is under constant development, and has gone through several updates during the time of this project. The latest version of the program used was Revision 1761.

3.2 Full grid-search location

For this project, we have used the full grid-search location method, in the location recipes in MStudio, to obtain locations within the study area. Later we have digitally manipulated the resulting figures to create a clearer presentation of the results, and to include the locations of all 11 shots in the same maps (Figure 11).

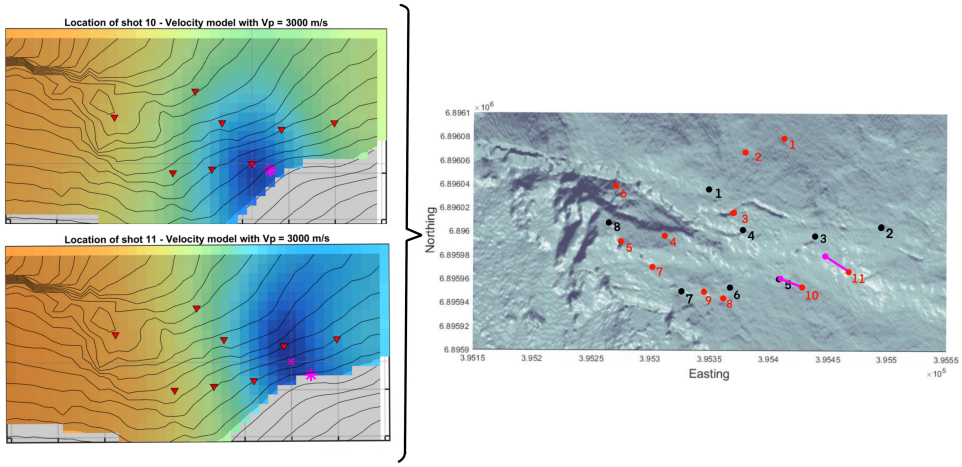

Figure 11: The colour-coded maps on the left are examples of the maps created in MStudio based on the full grid-search location method. The colours are derived from a misfit function, and indicates the probability of a location in each grid-cell. The geophones are marked with red triangles, the true location of the shots are marked with pink stars and the obtained location is marked with pink crosses. The map on the right is made by layering the left figures, making them transparent, and manually drawing the locations onto the map of the study area. To achieve this result we have used the digital drawing program ProCreate. Here the geophones are marked with black points, the shots are marked with red points and the obtained locations of the shots are marked with pink points. The pink lines show the direct path between the true and calculated locations.

The goal of a full grid-search is to check how well each grid-cell satisfies the problem statement. In this case, each cell of the grid is a potential location. The algorithm checks how realistic each location is, with respect to the observations. This is done through the computation of a misfit value. The misfit is obtained by systematically calculating the traveltime residuals (the difference between observed seismic wave picks and theoretical picks $|t_{observed} - t_{theoretical}|$) for each grid-cell, and combining them into a single value. The goal in our case is to minimize the misfit. The grid-cells are colour-coded according to the misfit value. The general colour spectrum goes from blue to orange. Blue signifies lower misfit values, while orange signifies higher misfit values. In other words, the location will be placed in the grid-cell with the darkest shade of blue. An example of colour-coded location maps is the two maps to the left in figure 11.

The misfit is calculated by the following least squares equation,

$$Misfit = \sqrt{\frac{1}{N_{picks}} \sum (\frac{t_{obs} - t_{theo} - t_{mean}}{\sigma_t})^2} \tag{1}$$

where t_{obs} are the observed and manually picked first arrivals, t_{theo} are the theoretical picks and t_{mean} is the mean traveltime residual, which is introduced to remove the absolute traveltime offset. The sum is over all available phase picks from all the geophones (N_{picks}) and σ_t is the expected measurement standard deviation (Wuestefeld et al., 2018).

For fine grid-resolutions or larger models, this technique is very thorough. However, it is computationally expensive. One can always expect a trade-off between computational time and the accuracy of the location. In other words, a higher grid-resolution will most likely give a more accurate result, but takes a longer time to run. It is also important to note that the accuracy depends on the precision of the seismic velocity model used. There is no need to use a grid-size smaller than the precision of the model. In this project, the size and resolution of the grid-cells are manageable, and the full grid-search location method runs smoothly.

3.3 Why locations based on homogeneous velocity models are ill-suited for the study area

The goal for this project is to create a velocity model which represents the area as accurately as possible. To kick-start the analysis of the data, we ran several tests using homogeneous velocity models. The process is explained in this section. However, as this section will demonstrate, the use of homogeneous velocity models provides a poor representation of the velocities in the study area.

In seismic processing one usually looks at P- and S-waves. One can also use sound-waves or surface-waves, but these are less common. The 11 calibration shots, which are the main source of data for this project, do not generate a clear S-wave component. This

is because very little shear movements occur in an explosion. Therefore we have mostly used the P-waves in our project. However, a strong sound-wave can be observed in the traces, where there are sudden changes in frequency or amplitude. These line up quite accurately with the sound-wave velocity of 330 m/s (the straight blue lines in Figure 4). As both the geophones and the test shots are located on the surface, the sound-waves can be quite helpful in the models to improve locations. This is because air is a homogeneous medium, which makes it a better fit for a homogeneous velocity model than the P-waves moving through the ground. Before running locations in MStudio, the first arrivals must be picked. Here, the first arriving P-waves are picked in blue, and the sound-waves are picked in orange (Figure 8). Even though the waves have been picked, they do not have to be included in the location process. One can choose to locate events using only the P-picks, only the sound-wave-pick or both. It is also possible to execute locations using only a selection of geophones.

The location algorithms based on homogeneous velocity models were used to locate the 11 calibration shots from 2006. All the location algorithms were run twice, once using only the P-picks, and once using both the P-picks and the sound-wave-picks. As the actual location of the shots are known, the root mean square errors (RMSE/RMS errors) of the locations obtained by the homogeneous velocity models are calculated using the equation:

$$RMSE = \sqrt{\frac{\sum_{i=1}^{n}(L_{Ai} - L_{Ci})^2)}{n}} \tag{2}$$

RMSE is the root mean square error, L_A are the actual locations of all calibration shots for the north, east and depth components and L_C are the locations calculated with the homogeneous velocity models. n represents the number of events. When working with the calibration shots, this number is 11 and is the same for all calculations. This is because all geophones were working at the time of recording, and all shots were registered by all geophones.

3.3.1 Homogeneous velocity models using only P-waves

Different homogeneous velocity models based only on P-waves have been used to locate the shots. RMS errors have been calculated for each case presented in figure 12. For comparison, the figure also includes a purple bar representing a velocity model based only on sound-waves. Excluding the sound-wave bar, the bar representing $3000m/s$ have the lowest error, with the ones for $3500m/s$ and $4000m/s$ close behind. In general, lower velocities give larger errors. As you can see, the bar representing the sound-wave, has a much lower RMS error. This is expected, as a homogeneous velocity model works better for representing air, than it does for representing heavily deformed rock masses.

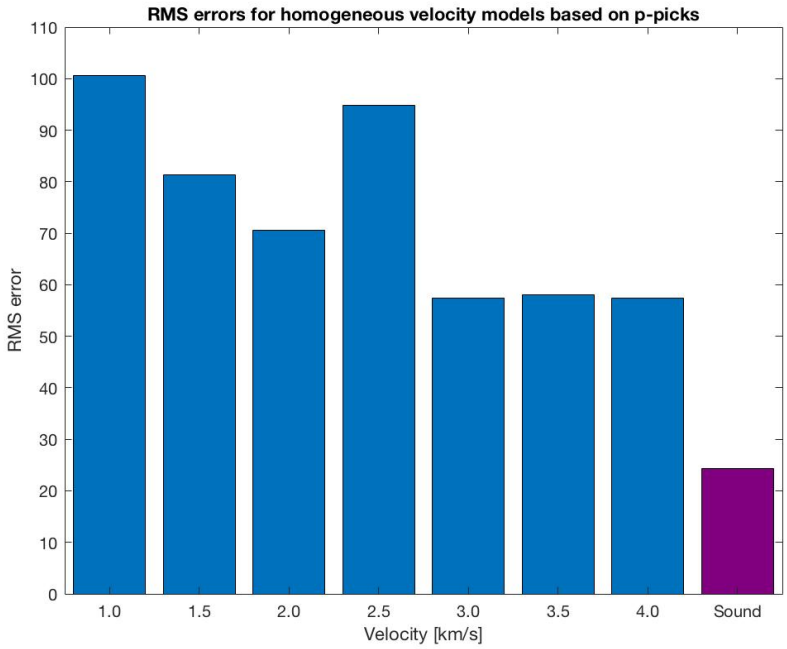

Figure 12: Total RMS errors of locations obtained by full grid-search locations based on homogeneous velocity models using only P-waves (blue), compared to the errors obtained by using only the sound-wave of 330 m/s (purple).

The distances between the true location of the shots and the locations derived from the model, are presented in table 3. They have also been decomposed in the north, east and depth component, to make the results easier to interpret. Distances above $50m$ have been

marked with red cells. This is because $50m$ are relatively large errors in an area that measures 400x200x200m. From this table, one can immediately see that the majority of the cells are red, which means that none of the homogeneous velocity models give accurate results.

	$V_p = 1500m/s$				$V_p = 2000m/s$			
	Total	North	East	Depth	Total	North	East	Depth
Shot 1	**24**	18	15	2	**24**	18	15	2
Shot 2	**58**	30	49	11	**58**	30	49	11
Shot 3	**97**	81	50	16	**101**	81	60	11
Shot 4	**236**	51	140	183	**225**	9	160	158
Shot 5	**190**	43	122	139	**160**	43	122	94
Shot 6	**97**	58	72	28	**87**	58	52	38
Shot 7	**192**	71	89	155	**197**	71	99	155
Shot 8	**131**	44	61	107	**90**	44	41	67
Shot 9	**169**	50	104	124	**126**	50	84	79
Shot10	**93**	57	50	54	**27**	7	20	16
Shot11	**111**	94	51	30	**57**	34	41	20
	$V_p = 2500m/s$				$V_p = 3000m/s$			
	Total	North	East	Depth	Total	North	East	Depth
Shot 1	**251**	62	155	187	**32**	18	25	7
Shot 2	**241**	50	131	196	**58**	30	49	11
Shot 3	**32**	19	10	24	**101**	81	60	11
Shot 4	**137**	101	40	83	**187**	49	160	83
Shot 5	**135**	17	108	79	**147**	23	122	79
Shot 6	**56**	52	12	17	**78**	58	22	48
Shot 7	**159**	69	61	130	**129**	71	59	90
Shot 8	**81**	44	49	47	**68**	44	31	42
Shot 9	**95**	50	56	59	**92**	50	64	44
Shot10	**202**	47	180	79	**27**	7	20	16
Shot11	**230**	44	211	80	**32**	14	21	20

Table 3: Errors for the locations of the 11 calibration shots, based on homogeneous velocity models using only P-waves with $V_p = 1500m/s, 2000m/s, 2500m/s$ and $3000m/s$. The bold numbers are the distances between the locations obtained by the models and the actual locations of the shots in meters. The distances have been decomposed in the north, east and depth directions. Cells containing errors above $50m$ are marked with red.

Figure 13 shows the locations obtained by homogeneous velocity models with $Vp = 1500m/s$ and $Vp = 3000m/s$. The pink lines show the direct path between the obtained and true locations. These correspond with the distances presented in table 3. The model with $Vp = 3000m/s$ was chosen because it is the homogeneous model giving the best results, and the model with $Vp = 1500m/s$ was chosen as it has been typically used for the area in previous studies. Among others, Fischer et al. (2019) used a homogeneous velocity model of $1500m/s$ in their study. The locations are generally inaccurate in both cases.

It is important to note that no locations obtained in MStudio will be placed outside the defined study area, as the model is constrained by its outer borders. The model is also constrained by the topography, and cannot place any locations above ground. In figure 13 one can see that a lot of the obtained locations (pink points) are placed at, or close to, the very edge of the study area. In cases like this, the locations obtained by the model might have been placed farther away from the actual position if the model allowed it, or if the defined study area was larger. In other words, the errors cannot exceed the size of the defined area, and it is important to interpret the results accordingly. A good example is the location of shot 1, which apparently have relatively low errors for both models with $Vp = 1500m/s$ and $Vp = 3000m/s$. This might be because the true location of shot 1 is close to the edge of the study area towards the north, and the location is constrained by the borders of the area.

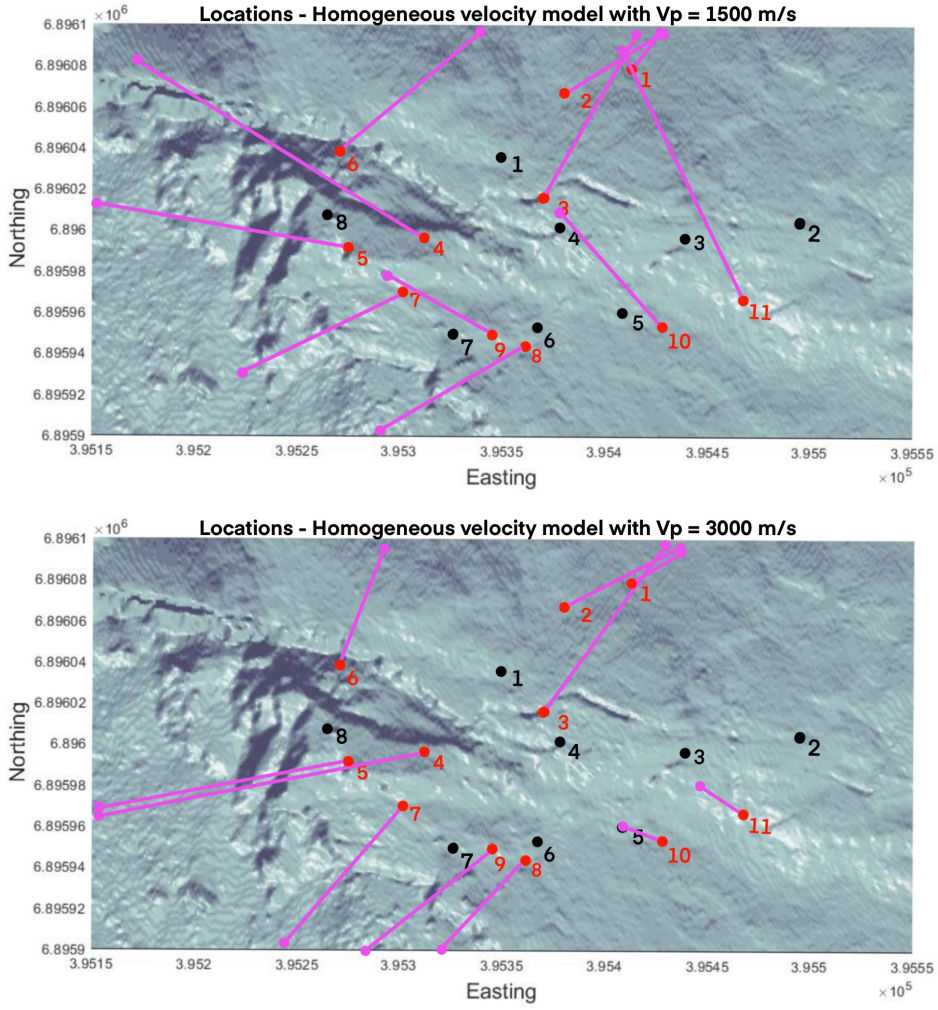

Figure 13: Location results obtained by homogeneous velocity models with $Vp = 1500m/s$ and $Vp = 3000m/s$. The black points show the location of the 8 geophones, the red points show the actual locations of the 11 calibration shots and the pink points show the locations of the shots obtained by the model. The pink lines show the direct path between the true and calculated locations of the shots.

The results, presented in the bar graph, table and figures (Figure 12 and 13 and Table 3), show that the locations obtained by homogeneous velocity models using only P-waves are generally inaccurate. All the locations are placed far away from their known positions. This indicates that homogeneous velocity models, using only P-waves, are ill-suited to represent the velocities in the study area.

3.3.2 Homogeneous velocity models using both P- and sound-waves

The locations based on models using both P-waves and sound-waves get much lower RMS errors than the models using only P-waves (Figure 14). In other words, using both types of waves in the same model gives better results. They are also generally superior to the result obtained using sound-waves only.

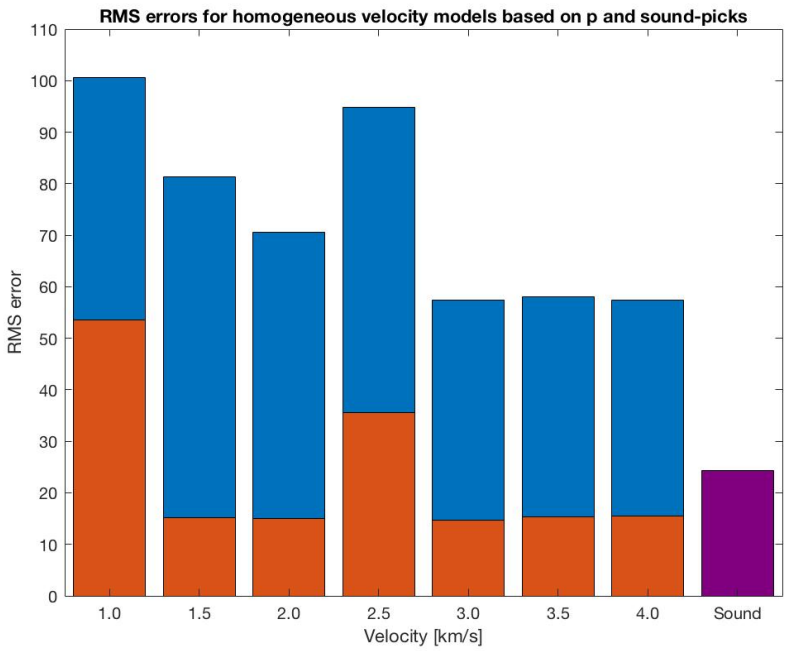

Figure 14: Total RMS errors obtained by velocity models using both P-wave picks and sound-wave picks (orange) and only P-wave picks (orange+blue), compared to the errors obtained by using only the sound-wave (purple)

The distances between the obtained shot locations and the true locations are presented in table 4. Again, the distances above $50m$ are marked with red cells, but here there are only a few outliers with errors larger than this. Compared to the previous table (3), these errors are much lower, meaning that the models produce much more accurate locations.

	$V_p = 1500m/s$				$V_p = 2000m/s$			
	Total	North	East	Depth	Total	North	East	Depth
Shot 1	**6**	2	5	2	**13**	12	5	2
Shot 2	**43**	10	39	16	**49**	20	39	21
Shot 3	**30**	21	20	6	**30**	21	20	6
Shot 4	**11**	11	0	3	**14**	11	0	8
Shot 5	**19**	17	8	4	**25**	17	18	1
Shot 6	**8**	2	8	2	**22**	22	2	2
Shot 7	**27**	9	1	25	**21**	9	11	15
Shot 8	**16**	16	1	2	**20**	16	9	8
Shot 9	**30**	30	4	1	**22**	20	6	6
Shot10	**21**	17	10	6	**23**	17	10	11
Shot11	**44**	34	11	25	**30**	24	11	15
	$V_p = 2500m/s$				$V_p = 3000m/s$			
	Total	North	East	Depth	Total	North	East	Depth
Shot 1	**62**	2	45	42	**23**	22	5	2
Shot 2	**69**	30	41	46	**41**	20	29	21
Shot 3	**29**	21	20	1	**23**	11	20	1
Shot 4	**36**	31	0	18	**10**	1	10	3
Shot 5	**25**	17	18	1	**25**	17	18	4
Shot 6	**43**	42	2	7	**23**	22	2	7
Shot 7	**25**	9	21	10	**23**	1	21	10
Shot 8	**11**	6	9	2	**20**	16	9	8
Shot 9	**32**	0	26	19	**33**	30	6	11
Shot10	**113**	3	110	24	**29**	17	10	21
Shot11	**119**	44	101	45	**18**	14	11	0

Table 4: Errors for the locations of the 11 calibration shots, based on homogeneous velocity models using P-waves with $V_p = 1500m/s$, $2000m/s$, $2500m/s$ and $3000m/s$ and sound-waves with $V_{sound} = 330m/s$. The numbers are the distances between the calculated locations and the actual locations in meters. Cells containing errors above $50m$ are marked in red.

The results obtained by using both the P- and sound-wave velocities in the location recipes, show that the calibration shots can be located quite accurately. However, the goal for the location model is to get accurate locations of incoming data from naturally occurring events, in addition to the calibration shots. Local and small-sized naturally occurring events may not generate clear sound-waves, which must be taken into account. To conclude, models combining P-and sound-waves are also ill-suited to represent the velocities in our study area.

3.3.3 Conclusions

There are no distinguishable sound- or S-waves in the naturally occurring events in the study area. Therefore, only P-waves can be used when locating naturally occurring events, which means that only P-wave velocities can be used in the final velocity model of the project. The results obtained from homogeneous velocity models based only on the P-waves, give unsatisfactory results, which means that a more accurate, heterogeneous 3D P-wave velocity model is needed.

The seismic velocities in the upper layers of the slope, are believed to be slow, due to heavy deformation. However, the homogeneous velocity model with higher velocities produce the best results. This might indicate that the velocities should be different in the upper and lower layers of the model, and that at least some of the waves propagate in the deeper layers.

4 3D velocity model building

A 3D heterogeneous velocity model is needed to locate events within the study area. This model is constructed in MatLab, and is based on the data obtained by the calibration shots, along with assumed and suggested geological structures from various scientific papers.

4.1 Velocity map

The distance between each calibration shot and each geophone, along with the traveltimes are known. This is used to calculate the mean velocities between each shot and each geophone (Figure 15). The actual wave paths are not necessarily straight lines, which means that the velocities on the map may not be accurate. They do, however, indicate a pattern in the velocities, showing how the velocities vary in some areas compared to others. We see that it is generally slower in the south-east corner, and faster in the north-west.

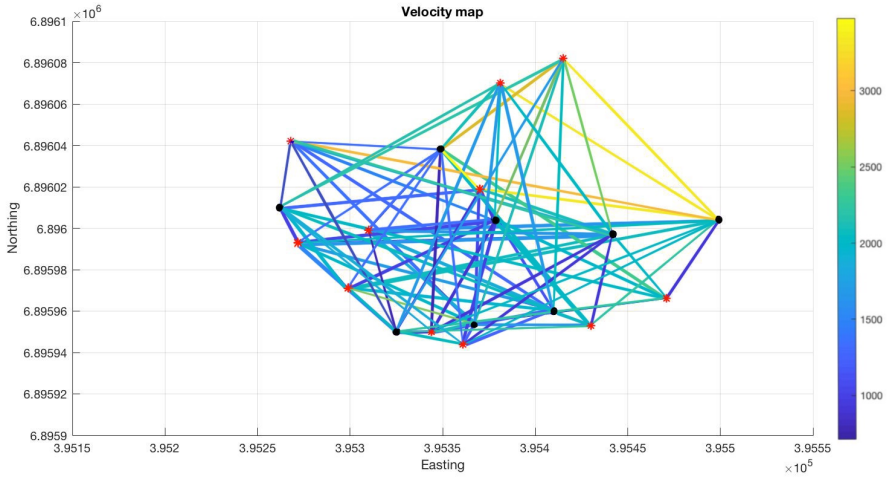

Figure 15: Velocity map of the study area. The colour of the lines represent the mean velocities $[m/s]$ between each of the shots and geophones, represented by red and black points respectively.

4.2 Modelling depth

The shots and geophones are all located on the surface, therefore there is very little information about how the geology in the study area looks like in depth. The first couple of steps in the 3D velocity model are solely based on data from the surface. These do not take vertical velocity changes into account. They only account for horizontal velocity changes, and have been modelled as 2D planes. However, MStudio cannot operate with 2D velocity models if they only account for the horizontal plane. In other words, information in depth is necessary to run the velocity models in the program.

The velocity maps in the xy-plane (horizontal) were duplicated in a layered model in the z-direction (vertical) (Figure 16). They were evenly distributed until the z-axis reached the desired depth for the study area. The number of layers depends on the horizontal model resolution, as the 3D-grid cells ideally should be cubes. Since the 2D planes were modelled with a resolution of 5x5m, the distance between the horizontal layers are also chosen to be 5m. The resolution of the 3D velocity models then becomes 5x5x5m. Due to the layering of equal 2D planes, the velocities vary in the xy-plane and are constant in the z-direction.

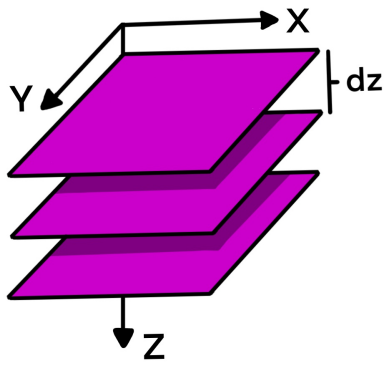

Figure 16: The velocity models created in the xy-plane are made into 3D by layering the planes along the z-axis until the desired depth is reached. This results in a velocity model with heterogeneous velocities in the xy-plane, and homogeneous velocities in the z-direction.

4.3 Grid-based velocity model

The initial heterogeneous velocity model is based on velocities from the velocity map (Figure 15), by segmenting the map, and using the approximated mean velocities for each segment. The waves most likely do not move in straight lines, like the figure shows. They might be refracted- or diving-waves. However, the figure gives an indication of how the velocities are located compared to each other. The velocity model is build up by four equally large grid-cells, each covering a quarter of the study area (Figure 17). The velocity map (Figure 15) shows a general trend of high velocities in the north-east, and low velocities in the south-west part of the study ares. Each grid-cell was filled with variables, representing the different velocities. 3D velocity models with different velocity values in the four parts, and homogeneous velocities in the z-direction, were used to locate the calibration shots in MStudio. The best location results were obtained from a model with $V_p = 1500m/s$ in the north-west section, $V_p = 2500m/s$ in the north-east section, $V_p = 1000m/s$ in the south-west section and $V_p = 1500m/s$ in the south-east section.

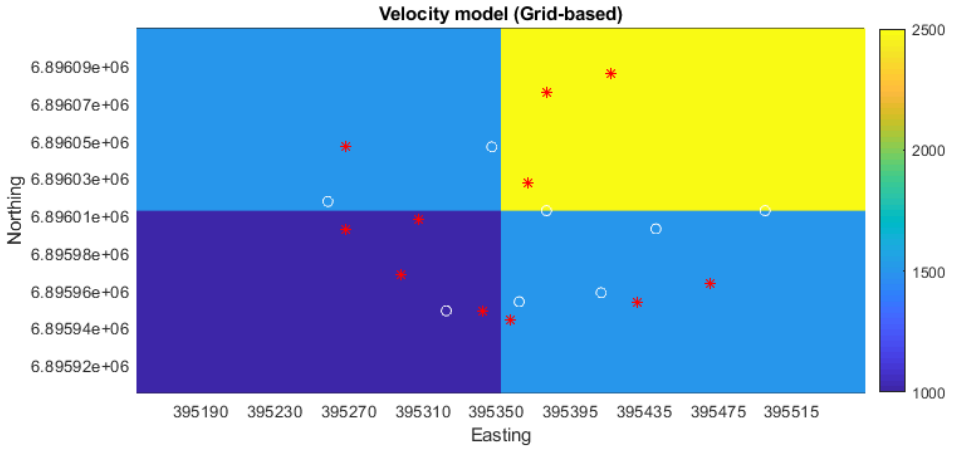

Figure 17: Grid-based velocity model based on the velocity map in figure 15. The model covers the same area as the defined study area. The colourbar represents velocities $[m/s]$, and the red and white points show the actual locations of the geophones and shots respectively.

Figure 18 shows the location results from MStudio when running a location recipe with

the best grid-based velocity model. No locations will be placed outside the defined study area. Although, several calculated locations have been placed on, or close to, the border of the model (Shots 1, 2, 3, 4, 5, 7 and 8). Because of the constraining borders, these locations might actually lie outside of the study area and thereby have an even larger error than what is apparent. Compared to the homogeneous velocity models, this one produces only slightly better results in general. Compared to the homogeneous velocity model of $v_p = 3000m/s$ the results are actually worse, as the homogeneous model gives better locations for shots 10 and 11. However, the grid-based model is based on velocities from actual measurements of the slope, and should be more geologically accurate than the homogeneous model.

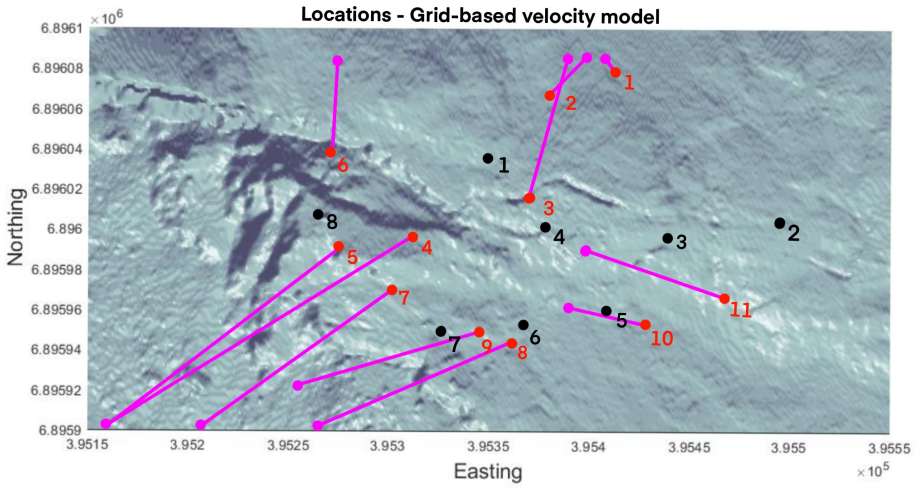

Figure 18: Location results obtained by the grid-based velocity model. The black points show the location of the 8 geophones, the red points show the actual locations of the 11 calibration shots and the pink points show the locations of the shots obtained by the model. The pink lines show the direct path between the true and calculated locations of the shots.

4.4 Fan-based velocity model

The grid-based model will be the base for the final model, but there is a lot of room for improvements. The 8 geophones and 11 calibration shots are all located in the center of the study area, which means that this is where we have the best information and res-

olution. A model with a higher resolution can be constructed in this area. This time it is based more directly on the mean velocity lines between the calibration shots and geophones from figure 15, rather than rough estimates as in the grid-based model.

Figure 20 shows a velocity model based on these mean velocity lines. As the lines themselves cover very little of the area, they were expanded by a fan shape between each shot and geophone. Where the shapes overlap each other, the mean value is calculated and used in that area. The velocities will be less accurate with increasing width of the fans. Because of this, they have a smaller impact on the model as the angle from the center line increases (Figure 19). The impact is regulated by multiplying the velocity in different sections of the fan with a decreasing number moving outwards from the center line. Different angles and decay constants were tested, until the best model was obtained. The model giving the best result has a 21 degree angle on each side of the center line, where a decay constant changes with 10 % for every 7 degrees.

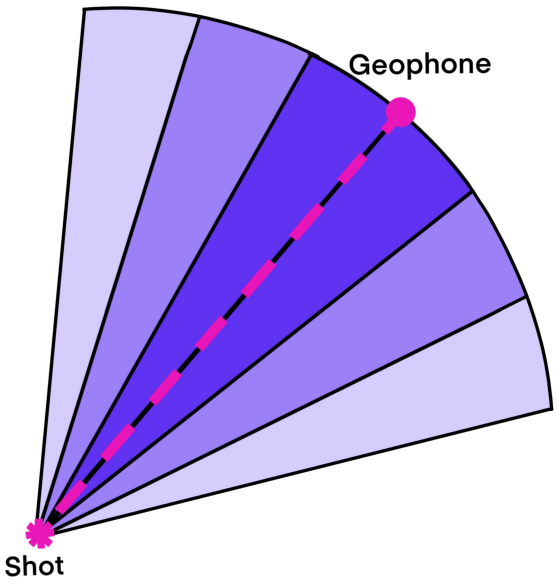

Figure 19: Example of a fan shape used in the fan-based velocity model. The shot and geophone are marked with a pink star and a pink point respectively. The center line is stippled between them. The intensity of the shape's colour is lighter farther away from the line, representing the decreasing impact of the velocities on the model.

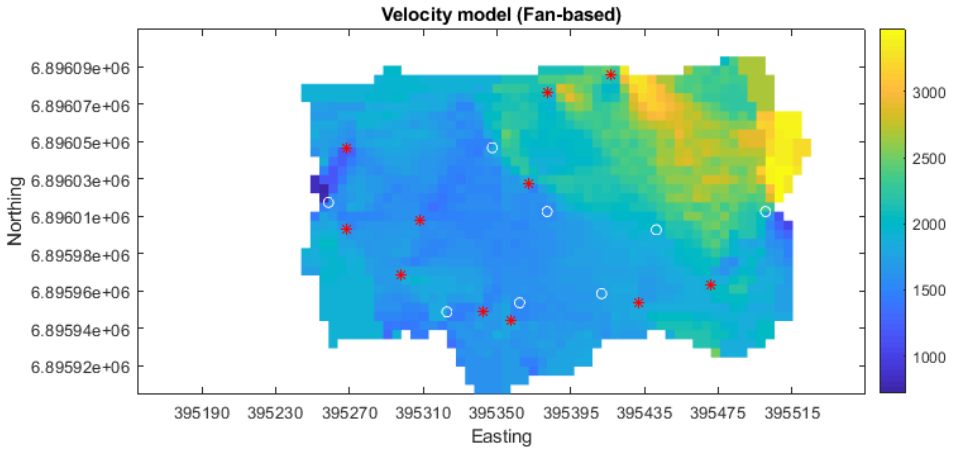

Figure 20: Velocity model based on fan shapes around the center lines between each shot and geophone. The colourbar represents velocities $[m/s]$. The red and white points show the locations of the geophones and shots respectively.

The fan-based velocity model only gives information in the center of the study area, and the outer areas are empty (Figure 20). The model can therefore not be used in a location recipe. It was combined with the previous model, by having the grid-based model as a background, filling the entire study area with velocities (Figure 21), before using it in MStudio.

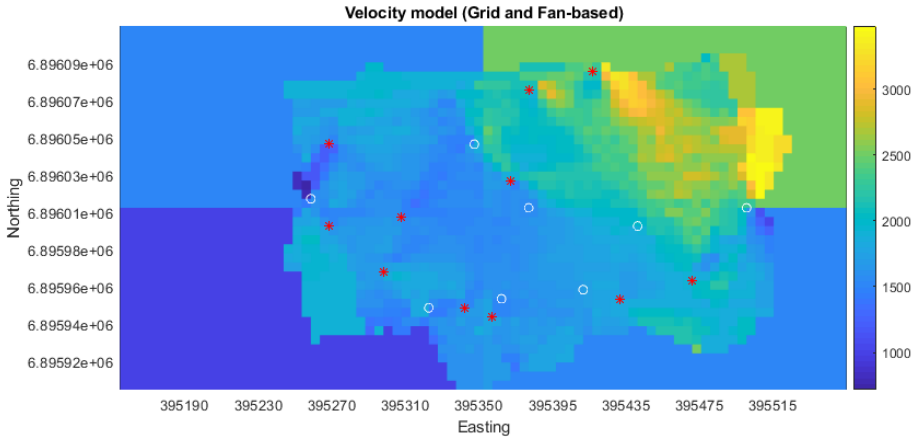

Figure 21: Combined velocity model based on both the grid-based model and the fan-based model. The colourbar represents velocities $[m/s]$. The red and white points show the locations of the geophones and shots respectively.

Figure 22 shows the location results from MStudio when running a location recipe with the combined fan-based velocity model. This model produces slightly better locations than the previous grid-based model. The distances between the calculated and actual locations are generally decreased, and fewer shots are located on the very edges of the study area. But the results are still not accurate. It is important to note that both this model, and the previous one is homogeneous in depth, and only takes horizontal velocity variations into account. They are also both based on the velocity map, with the mean velocities between each shot and geophone. Because the Åknes rock slope is heavily deformed at its surface, it is likely that the waves move faster further down, and will not necessarily follow the direct paths. It might therefore be necessary to include some velocity variations in the z-direction of the 3D velocity model to obtain better location results.

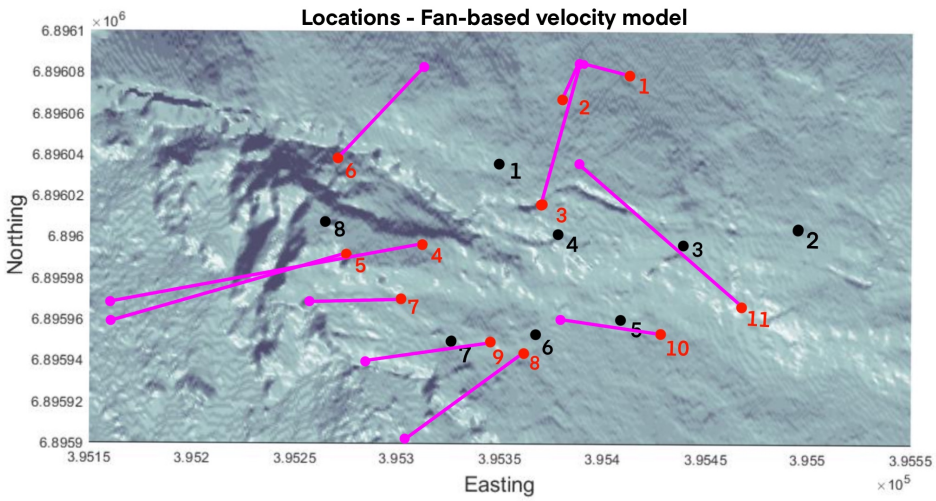

Figure 22: Location results obtained by the fan-based velocity model. The black points show the location of the 8 geophones, the red points show the actual locations of the 11 calibration shots and the pink points show the locations of the shots obtained by the model. The pink lines show the direct path between the true and calculated locations of the shots.

4.5 Velocity increase with depth

Although the geology at Åknes is mostly uncertain in depth, it is still possible to make the model more complex in the z-direction. This is based on the assumption that seismic velocities generally increase with depth. We can assume this because the surface of the slope is much more subjected to deformation and erosion than what is probable in deeper areas. A fractured rock mass with lower strength displays lower seismic velocities than a solid rock mass (Boadu, 1997).

To introduce a velocity increase with depth into the 3D velocity model, each xy-plane was multiplied with a gradient. Several increase rates of the gradient were tested for the model. The best fitting velocity increase was based on the natural logarithm of e, giving numbers increasing from 1 at the top of the model, to 1.6 at the bottom of the model. This gives a velocity range from approximately $V_p = 800m/s$ to $V_p = 5500m/s$, which lies within the spectrum of realistic seismic velocities in gneiss. The addition of this feature improved the locations compared to the model without velocity increase. Figure 23 shows

three sections of the model combining the grid-based and the fan-based velocity models with gradually increasing velocities with depth.

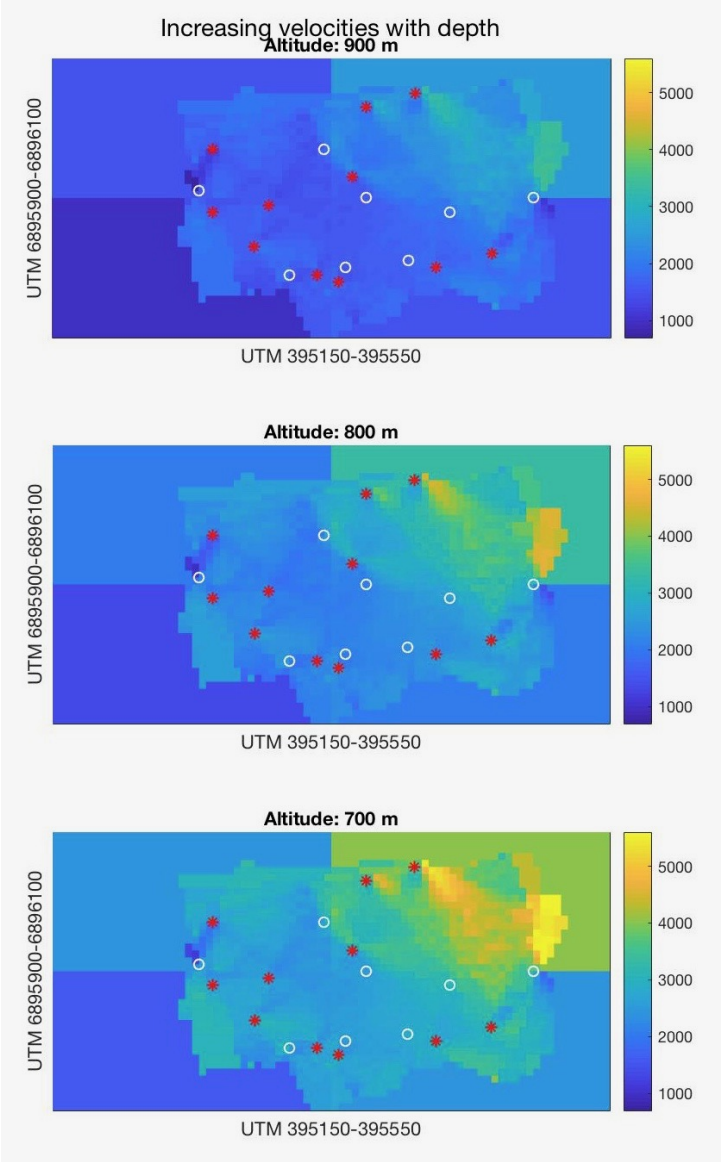

Figure 23: Three sections of the model with increasing velocities with depth. The top panel is located at an altitude of $900m$ above sea level, the middle at $800m$ and the bottom at $700m$. In other words, the top, middle and bottom planes of the defined study area. The colourbar represents velocities $[m/s]$. The red and white points show the locations of the geophones and shots respectively. These are actually located on the surface.

With this model, most of the errors have become smaller compared to the results from previous steps (Figure 24). This shows that the locations are affected by the velocities in depth, and models based purely on the velocities close to the surface cannot represent the area by themselves. However, not all locations have improved, as shots 7 and 9 have become less accurate. The locations are not yet very accurate, and the model needs more updates.

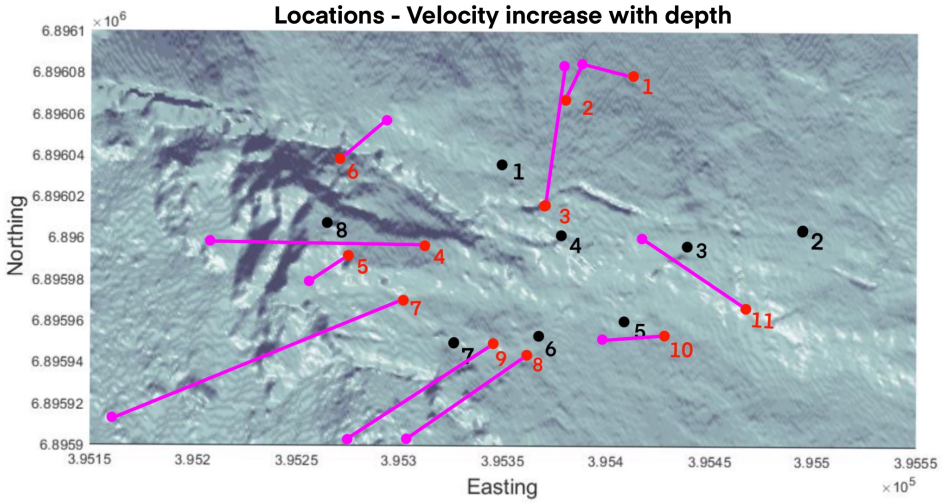

Figure 24: Location results obtained by the velocity model with increasing velocities in depth. The black points show the location of the 8 geophones, the red points show the actual locations of the 11 calibration shots and the pink points show the locations of the shots obtained by the model. The pink lines show the direct path between the true and calculated locations of the shots.

Another test model, based on a gradient resulting in much higher velocities, actually produced more accurate location results. However, the maximum velocities for this model exceeded $10,000 m/s$ which is unrealistic in gneisses. Therefore this model was discarded, and the model with a smaller velocity increase was used instead, even though it had a less accurate result. This improvement in location results with very high velocities in depth, might suggest that a high velocity zone is located somewhere beneath the rock slope. This might confirm the existence of the assumed sliding plane separating the unstable rock slope from the rest of the mountain.

4.6 Sliding plane

A sliding plane is assumed to separate the unstable part of the Åknes site from the undeformed part the mountain. The true location of this plane is unknown, although, several depths have been suggested. Blikra et al. (2013) suggests a depth of $50m$, and Kveldsvik (2008) suggests a depth of $120m$, which are both tested in this model. The geology underneath the sliding plane is unknown. However, one can assume that it is less deformed than the moving slab and will consist of a more homogeneous material. Therefore it should have a higher seismic velocity.

The shots and geophones are all located on the surface of the rock slope. The maximum difference in altitude between the geophones are $110m$. Therefore, modelling a sliding plane at a depth of $120m$ (and less) is enough. The first arriving waves would most likely not reach these greater depths. However, a larger study area based on more information, could make it possible to operate at greater depths, and test other suggestions.

The sliding plane was implemented in the model by using the defined topography. A file, containing coordinates of the topography, with a grid-size of 5x5x5m, the same resolution as the 3D model, was used as a base for the sliding plane. All points in the topography matrix were moved down to the desired depth of $50m$ and $120m$. Then the previous velocity model was run through an 'if-loop', checking if each point is located above or underneath the sliding plane. If the point is located above, it does not change, but if it is located under, it is given the value of a variable representing the velocity of undeformed gneiss. $V_p = 5000m/s$ was chosen to represent the undeformed gneiss underneath the sliding plane. The velocity model with a sliding plane at a depth of $50m$ is presented in Figure 25.

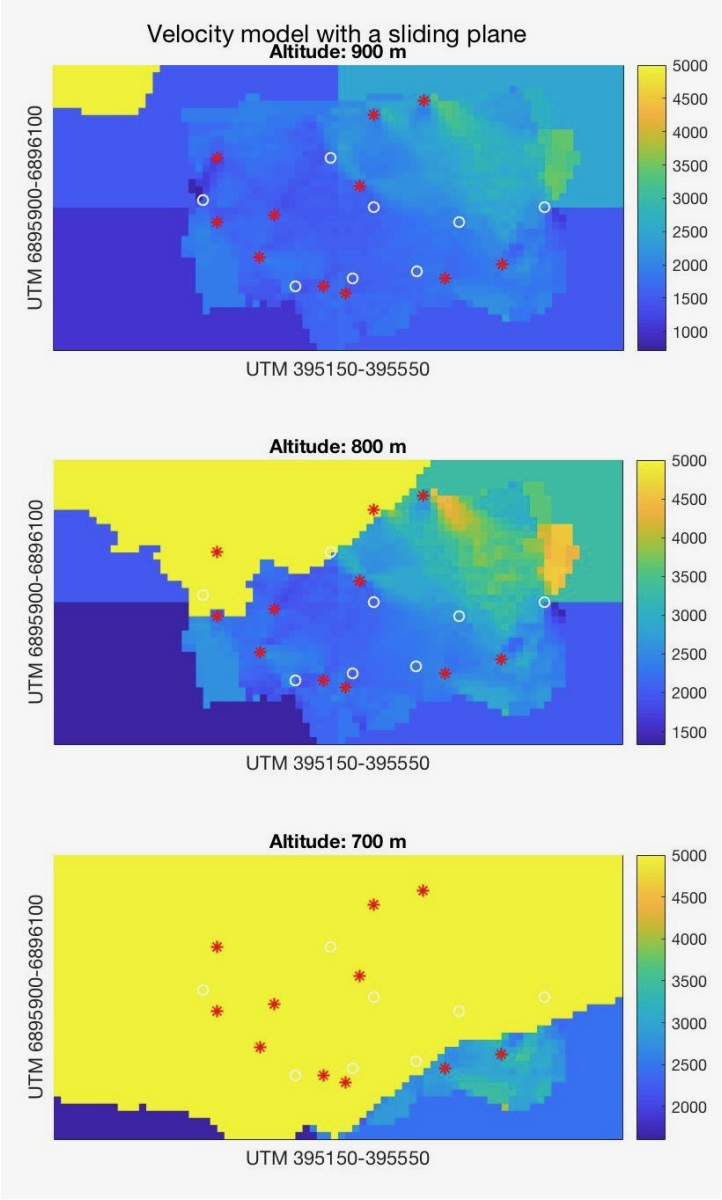

Figure 25: Three sections of the velocity model with a Sliding Plane at a $50m$ depth compared to the surface. The top panel is located at an altitude of $900m$ above sea level, the middle at $800m$ and the bottom at $700m$. In other words, the top, middle and bottom planes of the defined study area. The colourbar represents velocities $[m/s]$. The red and white points show the positions of the shot and geophones respectively. These are actually located on the surface.

Both models containing sliding planes show great improvement compared to the previous results (Figures 26 and 27). The model with a sliding plane at 120 m still places shot 1, 2

and 3 close to the edge of the defined model, while the rest of the locations are generally improved. The model with a sliding plane at a 50 m depth produces improved locations for almost all shots, and is the one that will be used in the final 3D velocity model for this project. However, shot 4 and 6, which are located in and close to the graben structure, still have relatively large errors. This suggests that the velocities around this area can be improved further.

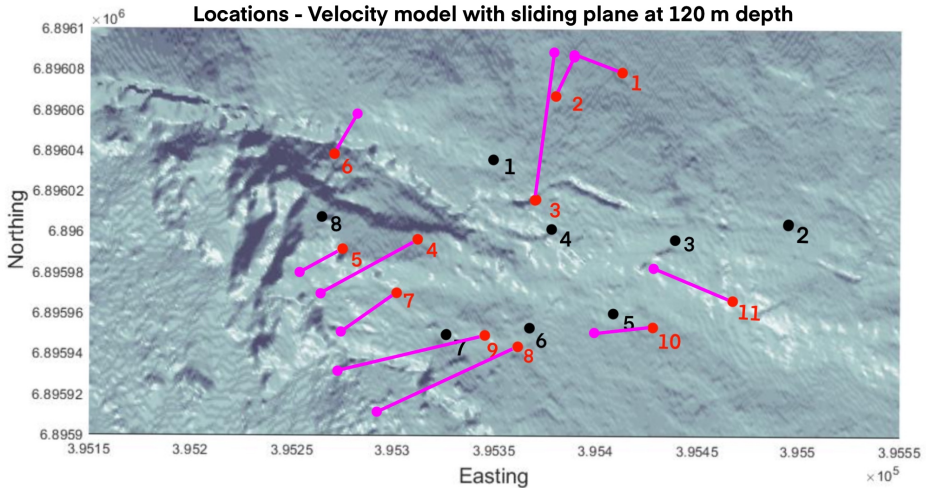

Figure 26: Location results obtained by the velocity model with a sliding plane at 120m depth. The black points show the location of the 8 geophones. The red points show the actual locations of the 11 calibration shots and the pink points show the locations of the shots obtained by the model. The pink lines show the direct path between the true and calculated locations of the shots.

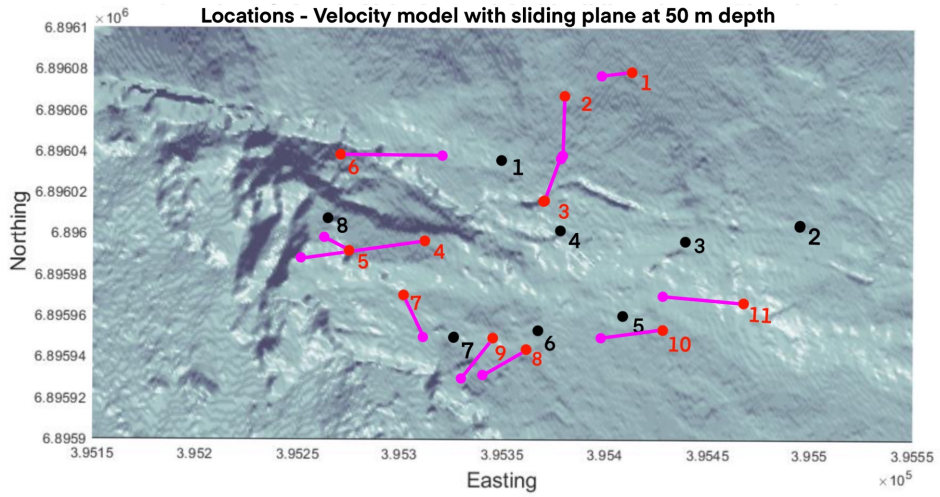

Figure 27: Location results obtained by the velocity model with a sliding plane at $50m$ depth. The black points show the location of the 8 geophones. The red points show the actual locations of the 11 calibration shots and the pink points show the locations of the shots obtained by the model. The pink lines show the direct path between the true and calculated locations of the shots.

4.7 Graben structure

A graben structure is located at the very top of the Åknes rock slope, which can be seen in figure 3 in section 2.2. As the upper part of the slope is subjected to extensional forces, the surface is filled with cracks and fractures in this area. It is safe to assume that this area will have lower seismic velocities than its surroundings. To implement this low-velocity area into the velocity model, the map of the study area was used. The graben structure can be observed in the maps, located just above geophone 8. Shots 4 and 6 are located inside and just outside this area. The best fitting shape for the low velocity zone is an ellipse, roughly covering the graben structure. This was done instead of having a shape perfectly covering the graben, as the low velocity area may include the immediate surroundings. Figure 28 shows the development of the graben model. The first panel shows the graben structure and the assumed surrounding low velocity area marked with a red ellipse. The following panels show this shape filled with black, and the rest of the figure is coloured with white. The black and white image is then imported into MatLab and converted into a matrix. As the image only consists of two colours, the cells of the corresponding matrix only consists of two different values. To implement the graben

structure, all the velocities inside the structure were changed and the velocities outside the structure remained unchanged. This was done by changing the number representing white with 1, and the numbers representing black with a number < 1. The matrix was resized to have the same resolution as the velocity model (Figure 29). It was then multiplied with the velocity model, only changing the velocities inside the low velocity area (Figure 30). The best results were obtained when the low velocity area was changed to half it's original velocity, by changing the numbers inside the black ellipse to 0.5.

It is uncertain how deep down the low velocity area should go. In this model it is not stopped, and follows the vertical direction as a cylinder. It is, however, subjected to the gradual velocity increase with depth, and is cut off by the sliding plane $50m$ beneath the surface along with the other features of the velocity model.

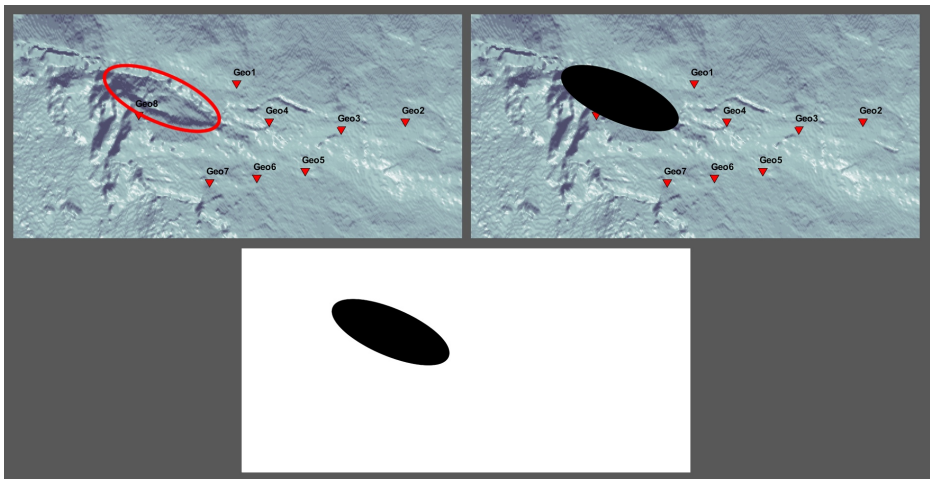

Figure 28: Three stages of creating the low velocity area surrounding the graben structure. The red ellipse shows the rough location of the graben structure, and the low velocity area. This shape is filled with black, and the background is filled with white. The image can now be imported into MatLab to be converted into a matrix.

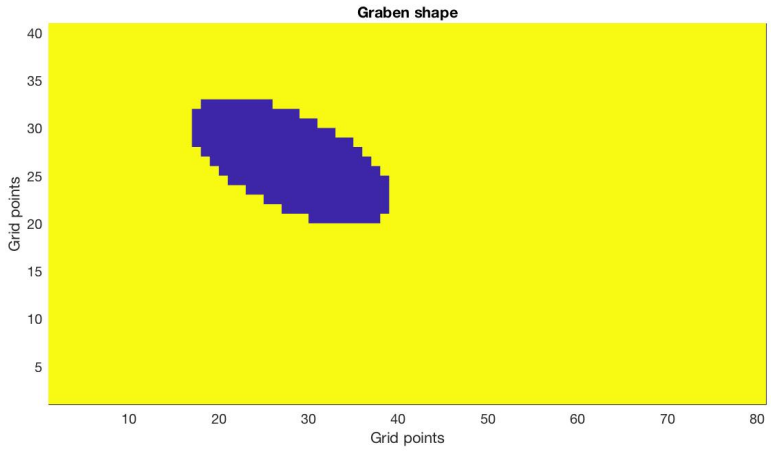

Figure 29: The black and white image, representing the graben structure and the surrounding low velocity area, have been converted into a matrix, with the same dimensions and resolution as the velocity model. It can now be merged with the model.

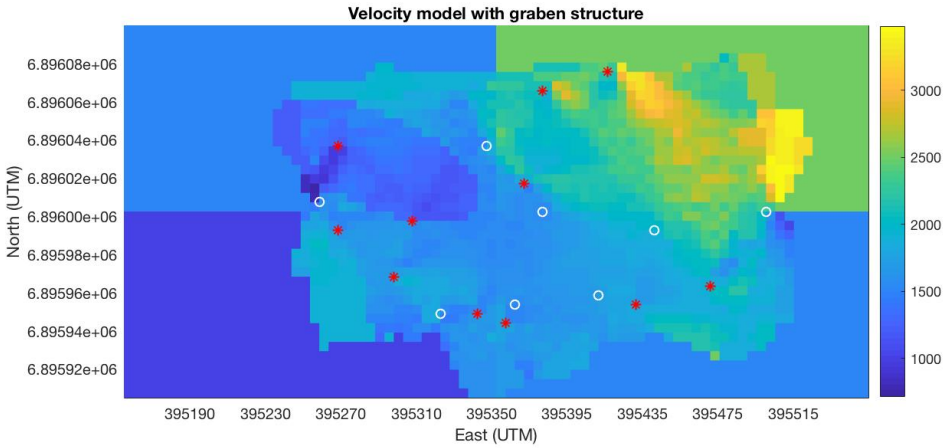

Figure 30: The velocity model with the graben structure. The colourbar represents velocities $[m/s]$.

The location results from this model are very similar to the previous results, as the only addition is the low velocity zone surrounding the graben structure. However, the lo-

cations affected by this area, specifically shots 4 and 6, have greatly improved (Figure 31).

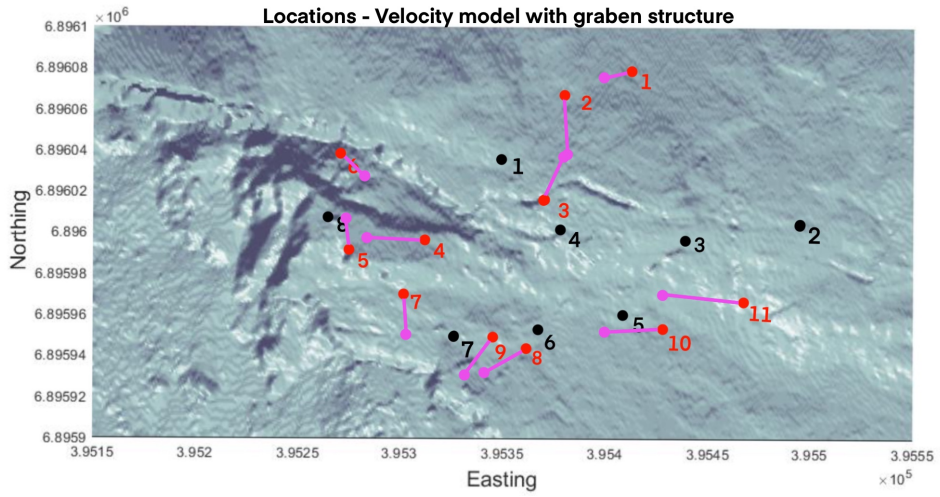

Figure 31: Location results obtained by the velocity model with a low velocity area defined by the graben structure. The black points show the location of the 8 geophones, the red points show the actual locations of the 11 calibration shots and the pink points show the locations of the shots obtained by the model. The pink lines show the direct path between the true and calculated locations of the shots.

4.8 The final 3D velocity model

The final 3D velocity model for this project is now obtained, including all the features described in previous steps. It includes the grid-based model, fan-based model and the low velocity zone determined by the graben structure as 2D planes. These are subjected to a velocity increase with depth, and are cut off by a sliding plane $50m$ beneath the surface. Figure 32 shows three layers of the model, describing how it changes with depth.

The final velocity model was used to locate the calibration shots. The obtained locations are presented in table 5. These numbers correspond to the pink points in figure 31. The true locations of the shots are presented in table 1 in section 2.4.

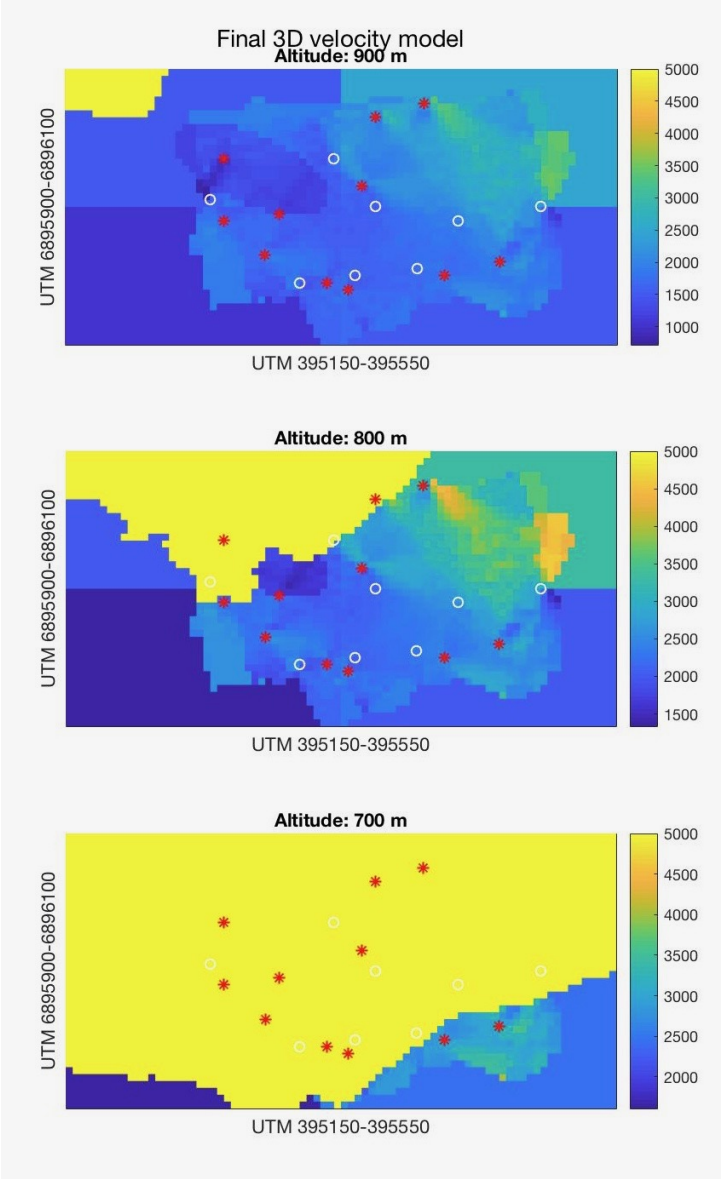

Figure 32: Three sections of the final 3D velocity model. The top panel is located at an altitude of $900m$ above the sea level, the middle at $800m$ and the bottom at $700m$. In other words, the top, middle and bottom planes of the defined study area. The colourbar represents velocities $[m/s]$.

	Northing (UTM) $[m]$	Easting (UTM) $[m]$	Depth (- altitude) $[m]$
Shot 1	6896080	395400	-860
Shot 2	6896000	395380	-850
Shot 3	6896040	395380	-850
Shot 4	6896000	395280	-855
Shot 5	6896010	395270	-870
Shot 6	6896030	395280	-870
Shot 7	6895950	395300	-800
Shot 8	6895930	395340	-775
Shot 9	6895930	395330	-770
Shot 10	6895950	395400	-760
Shot 11	6895970	395430	-760

Table 5: The locations of the 11 calibration shots from 2006, calculated with the final velocity model.

4.8.1 The development of the model

Each added feature or update of the final 3D velocity model gave improved location results when locating the calibration shots. The total RMS errors calculated with equation (2) are presented in figure 33. It is important to note that the sliding plane at $120m$ depth is not used in the final model. It was discarded and the sliding plane at $50m$ depth was used instead.

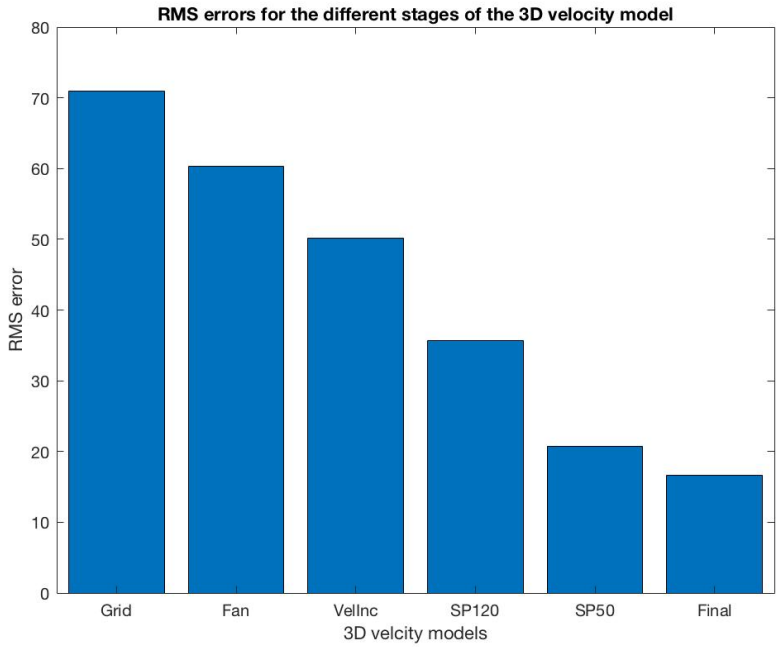

Figure 33: Total RMS errors for locations obtained by the different steps of the final 3D velocity model.

Table 6 shows the distance in meters from the locations obtained by the various features and steps of the 3D model and the true locations of the 11 calibration shots. These distances represent the lengths of the pink lines in the location maps from all the steps of the model (Figures 18, 22, 24, 26, 27 and 31). The distances have also been decomposed in the north, east and depth directions. This makes it easier to see how accurate the models are, and in which directions the potential outliers might be. It includes the error distances in the z-direction, which cannot be seen in the figures. Cells containing distances above $50m$ have been marked in red, as they represent relatively large errors, considering that the study area is only 400x200x200m. The easiest way to observe the positive development of the model, is to note the decrease in the number of red cells for each step. The final model, where the graben structure has been implemented, has no errors above $50m$.

	Grid-based model				Fan-based model			
	Total	North	East	Depth	Total	North	East	Depth
Shot 1	**10**	8	5	3	**29**	8	25	13
Shot 2	**28**	20	19	1	**22**	20	9	4
Shot 3	**80**	71	30	21	**78**	71	20	26
Shot 4	**233**	99	160	138	**207**	29	160	128
Shot 5	**200**	93	122	129	**140**	23	112	79
Shot 6	**56**	48	2	28	**70**	48	42	28
Shot 7	**152**	71	89	100	**141**	71	39	115
Shot 8	**126**	44	101	62	**97**	44	61	62
Shot 9	**130**	50	104	59	**103**	50	64	64
Shot10	**41**	7	40	4	**41**	7	40	6
Shot11	**61**	14	51	30	**63**	34	51	15

	Velocity increase with depth				Sliding Plane at 120m			
	Total	North	East	Depth	Total	North	East	Depth
Shot 1	**29**	8	25	13	**29**	8	25	13
Shot 2	**22**	20	9	4	**22**	20	9	4
Shot 3	**78**	71	10	31	**78**	71	10	31
Shot 4	**118**	1	110	43	**65**	19	60	18
Shot 5	**29**	13	22	14	**29**	13	22	14
Shot 6	**40**	18	22	28	**40**	18	22	28
Shot 7	**182**	61	149	82	**85**	41	39	60
Shot 8	**78**	44	61	22	**78**	44	61	22
Shot 9	**123**	50	74	84	**98**	50	64	54
Shot10	**34**	3	30	16	**34**	3	30	16
Shot11	**62**	34	51	10	**64**	34	51	20

	Sliding Plane at 50m				Final velocity model			
	Total	North	East	Depth	Total	North	East	Depth
Shot 1	**17**	2	15	8	**17**	2	15	8
Shot 2	**32**	30	1	11	**32**	30	1	11
Shot 3	**26**	21	10	11	**26**	21	10	11
Shot 4	**61**	9	60	2	**31**	1	30	7
Shot 5	**15**	7	12	6	**20**	17	2	11
Shot 6	**52**	2	52	3	**17**	12	12	2
Shot 7	**31**	21	11	20	**29**	21	1	20
Shot 8	**25**	14	21	3	**25**	14	21	3
Shot 9	**31**	20	14	19	**31**	20	14	19
Shot10	**34**	3	30	16	**34**	3	30	16
Shot11	**44**	4	41	15	**44**	4	41	15

Table 6: Errors for the location of the 11 calibration shots, based on the 3D velocity models. The numbers are the distances between the calculated locations and the actual locations in meters. The distances have been decomposed in the north, east and depth directions. Cells containing errors larger than $50m$ have been marked in red.

4.8.2 Traveltime tables

Traveltime tables are derived from the final velocity model before the locations were carried out. This is done directly in MStudio, using the fast-marching algorithm. In this case, 8 traveltime tables are derived, each centered around one of the geophones in the study area. Figure 34 show the traveltime tables centered around geophones 1, 2, 6 and 8. These geophones were chosen as examples as they are farthest apart, and on the edges of the seismic network. All figures are shown in a map view, showing how the wavefronts move through the modelled heterogeneous medium at the surface.

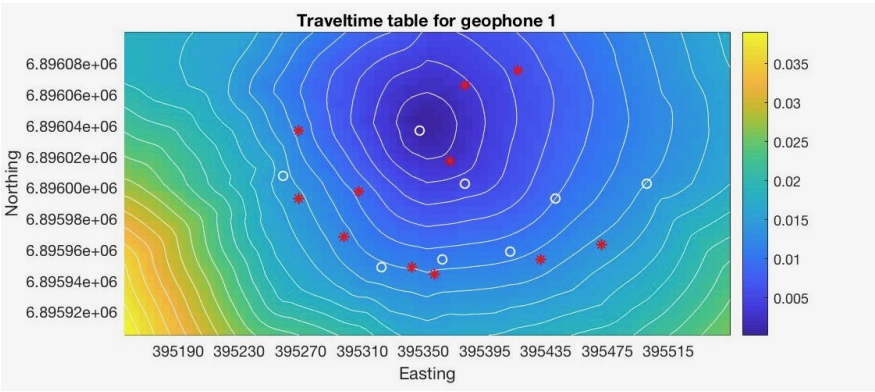
Traveltime table for geophone 1
Northing
6.89608e+06
6.89606e+06
6.89604e+06
6.89602e+06
6.89600e+06
6.89598e+06
6.89596e+06
6.89594e+06
6.89592e+06
395190 395230 395270 395310 395350 395395 395435 395475 395515
Easting
0.035
0.03
0.025
0.02
0.015
0.01
0.005

(a)

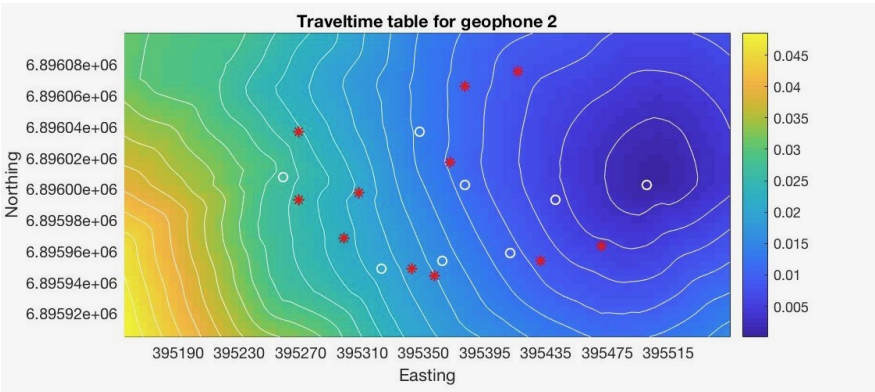
Traveltime table for geophone 2
Northing
6.89608e+06
6.89606e+06
6.89604e+06
6.89602e+06
6.89600e+06
6.89598e+06
6.89596e+06
6.89594e+06
6.89592e+06
395190 395230 395270 395310 395350 395395 395435 395475 395515
Easting
0.045
0.04
0.035
0.03
0.025
0.02
0.015
0.01
0.005

(b)

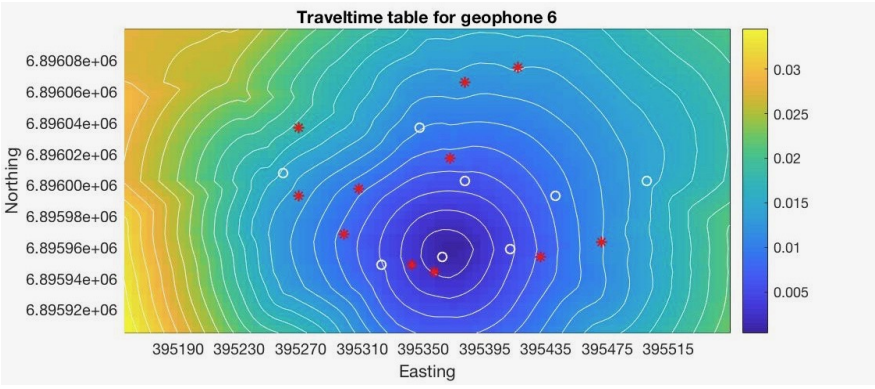
Traveltime table for geophone 6
Northing
6.89608e+06
6.89606e+06
6.89604e+06
6.89602e+06
6.89600e+06
6.89598e+06
6.89596e+06
6.89594e+06
6.89592e+06
395190 395230 395270 395310 395350 395395 395435 395475 395515
Easting
0.03
0.025
0.02
0.015
0.01
0.005

(c)

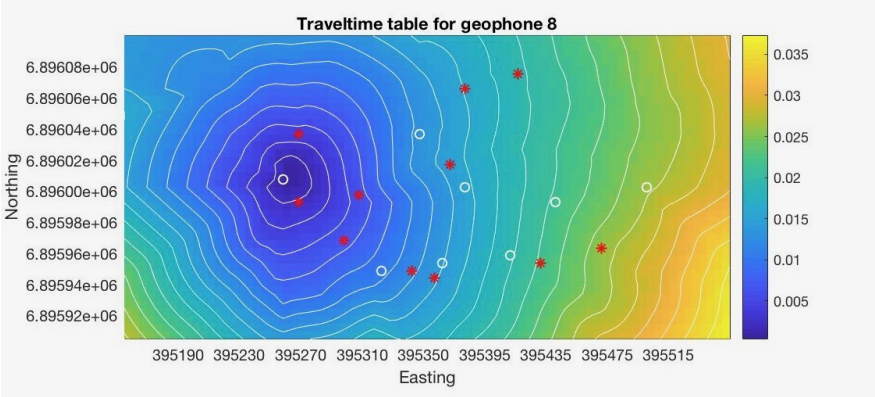

(d)

Figure 34: Traveltime tables derived from the final velocity model. The tables are viewed from the xy-plane, and shows the upper layer of the model. The white circles show the position of the geophones and the red stars show the positions of the shots. The colour bar shows time $[s]$. The figure was created using a script by Raanes (2011).

5 Locating naturally occurring seismic events

The final 3D velocity model now gets satisfactory results when locating the 11 calibration shots from 2006. The maximum error is $44m$ for the location of calibration shot 11 (Table 6), which is not perfect. However, the model will still be useful for estimating locations.

When manually updating the model by implementing features, there is no limit to how much the model can be updated. However, to get an accurate representation of the geology in the study area, only assumed or suggested geological features should be taken into account. It should be possible to construct a model that perfectly locates the 11 shots. But these are located on the surface, and act differently than natural events. Therefore it is important to note that a model perfectly representing the velocities for the shots, might not work as well for natural events. In other words, it is more important to make a model which is geologically realistic than a model that just reproduces perfect locations for a planned seismic experiment (the calibration shots).

5.1 Local events

The study area defined for this project is located at the upper part of the Åknes rock slope. As this area displays the highest rate of movement, one can expect much seismic activity here. The Åknes rock slope covers approximately $1km^2$, a much larger area than the $0.08km^2$ area modeled here. Even though one can expect frequent events within the study area, there will of course also be seismic events located outside of this area.

Four natural local events were picked at random to test how well the model works with natural data. The quality and signal-to-noise ratio vary from event to event. However, all events display clear peaks on most geophones, making it possible to pick arrival times. As mentioned previously, several geophones have been destroyed (and repaired) during the years. Because of this some geophones are only showing noise in the traces, depending on the time of recording. In these cases, the locations have been carried out using fewer geophones. This might affect the location results. These geophones were out of order for

the following cases: (a) geophone 5, (b) geophones 5, 7 and 9, (c) none and (d) geophone 7 (Figure 35).

The true locations of these events are unknown, meaning that there is no way of testing how accurate the calculated locations are (Figure 36). Events (a), (b) and (c) have been located within the geophone network. Local events in the study area are very likely to be a product of movement along the sliding plane. In other words, we expect the events to be located approximately $50m$ below the surface. However, event (a) and (b) are both located on the surface. Event (c) is located at a depth of approximately $40m$ (Figure 37), which is closer to what we would expect. However, as these are unknown events, we cannot tell which depth their true locations should be. The last event, (d), is located on the very edge of the defined study area. This location is especially uncertain as its true location might actually be outside of the study area.

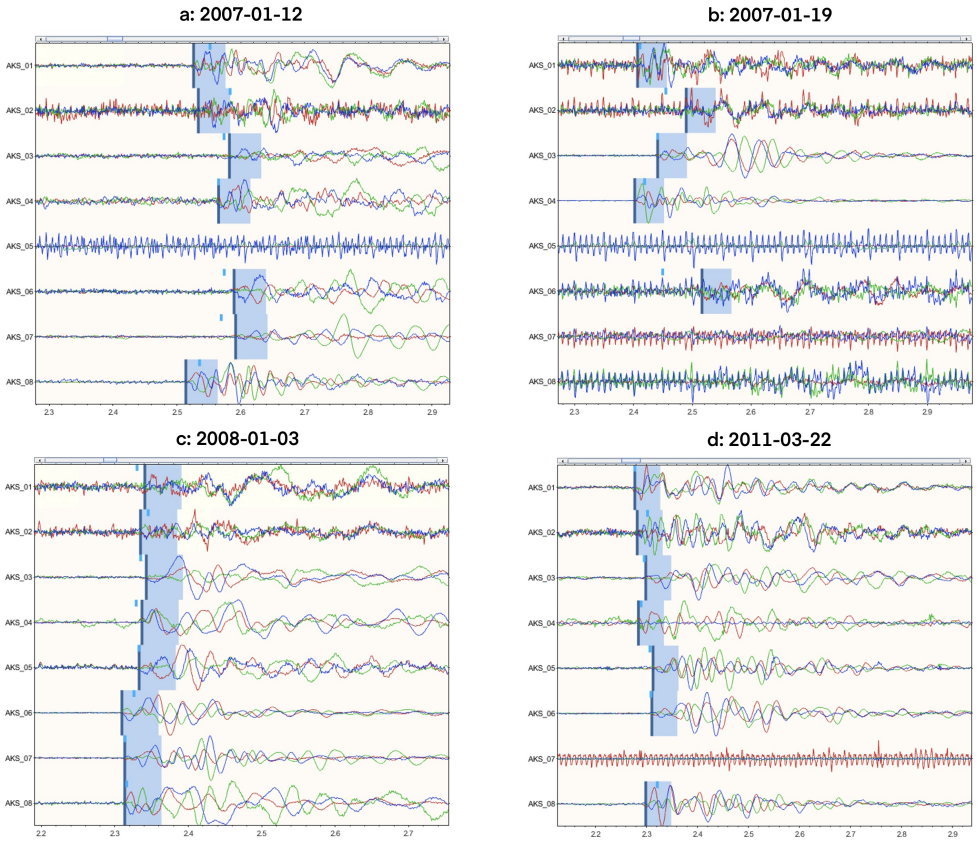

Figure 35: Data from local events from 2007, 2008 and 2011 viewed in WaveLab. The blue vertical lines show the first arrivals picked from the working geophones. The vertical axis show the geophone numbers and the horizontal axis show the time $[s]$.

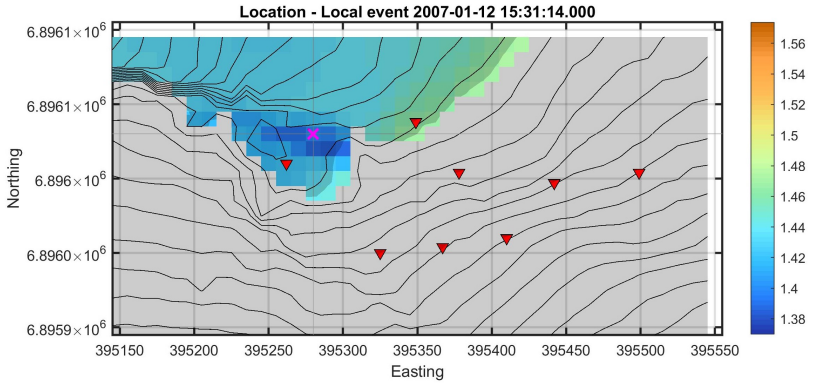
Location - Local event 2007-01-12 15:31:14.000
Northing
Easting
6.8961×10^6
6.8961×10^6
6.896×10^6
6.8960×10^6
6.8959×10^6
395150
395200
395250
395300
395350
395400
395450
395500
395550
1.56
1.54
1.52
1.5
1.48
1.46
1.44
1.42
1.4
1.38

(a)

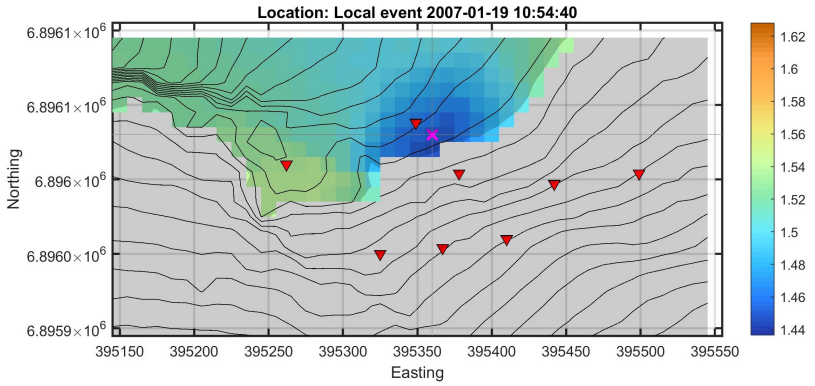
Location: Local event 2007-01-19 10:54:40
Northing
Easting
6.8961×10^6
6.8961×10^6
6.896×10^6
6.8960×10^6
6.8959×10^6
395150
395200
395250
395300
395350
395400
395450
395500
395550
1.62
1.6
1.58
1.56
1.54
1.52
1.5
1.48
1.46
1.44

(b)

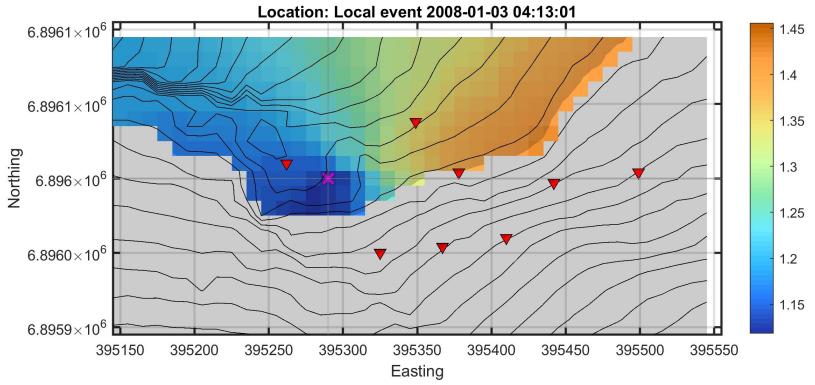
Location: Local event 2008-01-03 04:13:01
Northing
Easting
6.8961×10^6
6.8961×10^6
6.896×10^6
6.8960×10^6
6.8959×10^6
395150
395200
395250
395300
395350
395400
395450
395500
395550
1.45
1.4
1.35
1.3
1.25
1.2
1.15

(c)

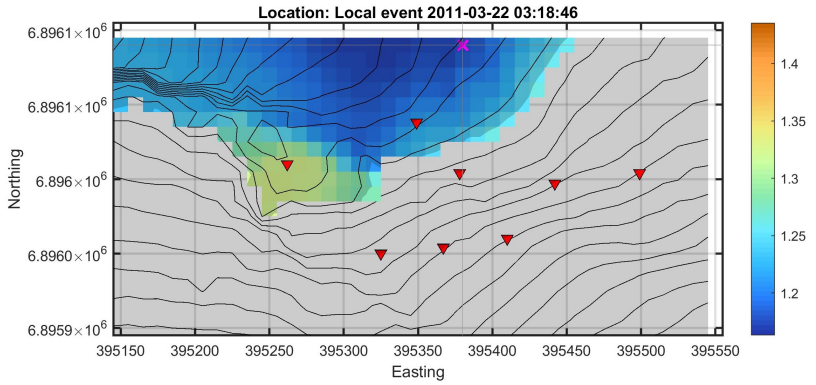

(d)

Figure 36: Location of four local events from 2007, 2008 and 2011. The pink crosses show the calculated locations. The red triangles show the placement of the geophones. The colourbar represent the misfit to the data obtained by the full grid-search location algorithm.

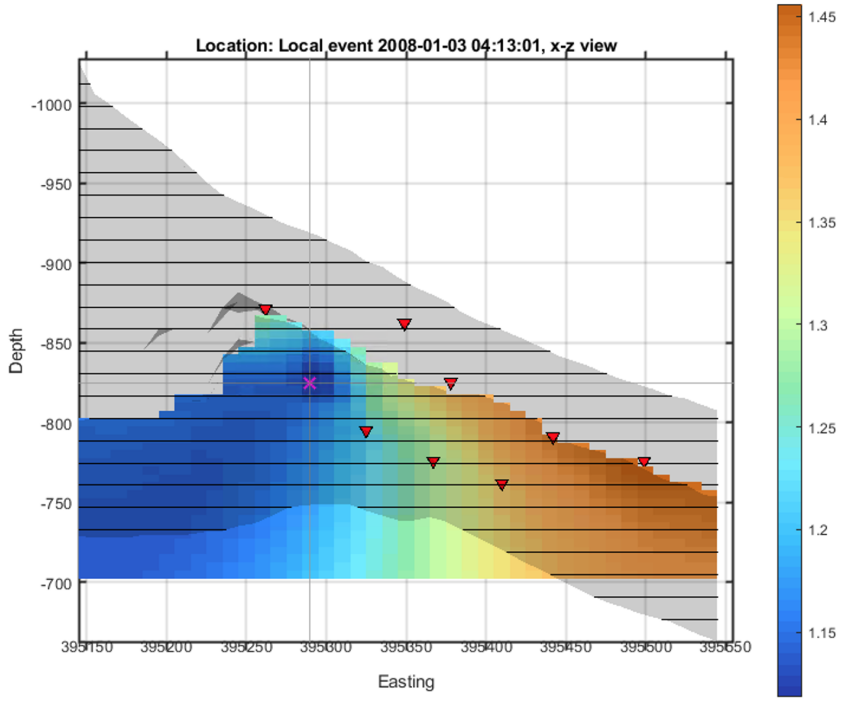

Figure 37: Location of the local event from 2008 (case (c) in Figure 36) viewed in the xz-plane. This angle shows the location in depth. The pink cross show the calculated location. The red triangles show the placement of the geophones. The colourbar represent the misfit to the data obtained by the full grid-search location algorithm.

5.2 Snow avalanche

There is no way of telling if the model shows the location of a local event accurately. Therefore we need another way to test the accuracy of velocity model. This was done by locating a snow avalanche. The chosen event damaged the cable of one of the geophones in the network. Even though the location of the event is not precisely known, one can assume an approximate location as it must have happened close to the geophone it affected.

It is important to note that locating events like snow avalanches or rockfalls might not be an easy task, as they are surface processes. These events last longer, have more noise and will often generate sound-waves. Therefore, the waveforms are complicated and more

difficult to interpret than shots or local events. However, it worked out in this case as the event had a strong recorded arrival on most geophones. When picking the arrivals for locating snow avalanches or rockfalls, one should generally not pick the geophones which have been destroyed in the scenario. This is because the events often happen too close in time to when the cables were damaged. This makes the data unreliable. In this case, a snow avalanche destroyed the cable for geophone 2. However, for this particular event, it is possible to pick the arrival detected by the affected geophone, as this pick corresponds to the beginning of the event, and the cable was damaged later. It can be possible to see whether or not one should pick the geophone in question by looking at the waveform. An important note that is also apparent in this case, is that the 3-component geophones in the seismic network register the components of the incoming waves separately. Geophone 4 registered much noise on its depth-component (blue trace in Figure 38). To get a clear pick, the data were only viewed for the north- and east-component when picking the arrival for this particular geophone. By the time of the event, geophone 7 was already out of order, and has not been used in the location (Figure 38).

Figure 39 shows the location of the snow avalanche which destroyed the cable for geophone 2. The location is placed very close to the affected geophone, which suggests that the location points out the right area. It is also located on the surface, which is what we expect for an event like this. However, since avalanches often affect large areas, the accuracy of the location could be overstated. An important observation regarding the accuracy of the location, is that there is a large area of uncertainty surrounding the obtained location. This is represented by the blue in the colour map (Figure 39).

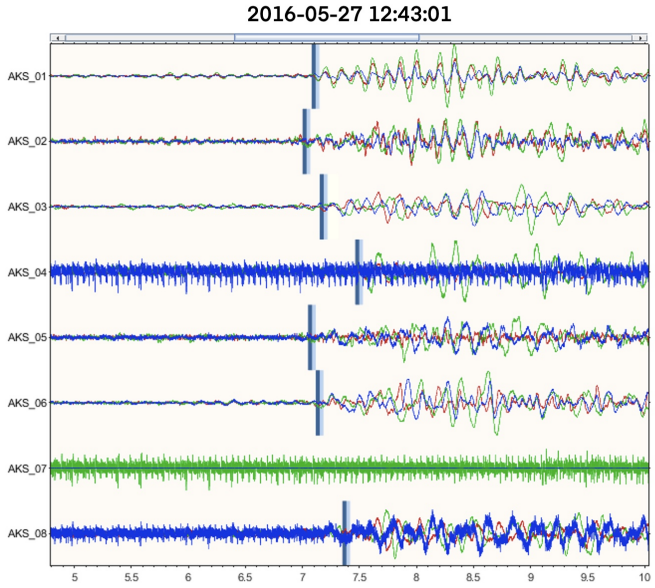

Figure 38: Data from an avalanche from the 27^{th} of May 2016. The picks are marked in blue vertical lines.

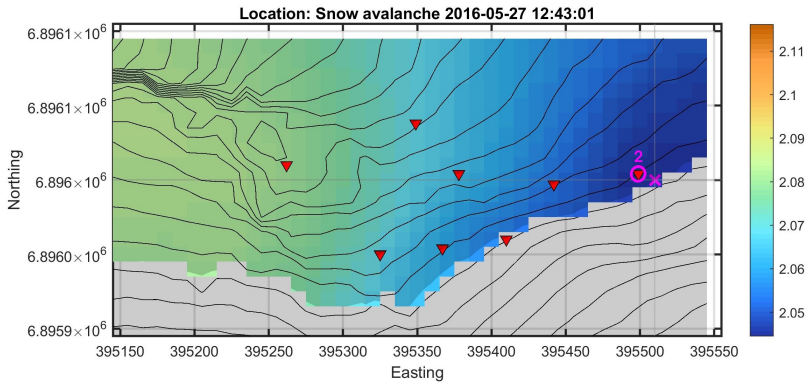

Figure 39: The location of an avalanche form 2016, marked by the pink x. The affected geophone (2), is marked by a pink circle. The colourbar represent the misfit to the data obtained by the full grid-search location algorithm. They are based on the residuals, where the lowest number represents the highest probability of a location.

5.3 Block collapse

The location of the snow avalanche indicates that the velocity model might be a good representation of the velocities in the area. However, snow avalanches often cover large areas. This means that even though the obtained location is close to where we assumed it to be, it is not a very precise observation. Therefore it might be better to look at a more defined event to check the accuracy of the model.

This is done by locating a block collapse from September 2012. The approximate location of this event is known, as it was observed by people working on the slope at the time. They reported that it happened close to geophone 3 at approximately 16:00. The block collapse was a result of an approximately $30m$ block detaching from the back scarp, and dropping a couple of meters (Fischer et al., 2019).

Several events were chosen to locate the block collapse. These events happened around the approximate time of the collapse, and can be assumed to be associated with the incident. The chosen events have nice waveforms, displaying clear peaks. This made the arrival times easy to pick. We decided to only use clear events, as we wanted any errors in the obtained locations to reflect the models accuracy, rather than human errors, resulting from unreliable arrival time picks.

Figure 40 shows the locations of the 8 chosen events. The bottom figure is a combination of the location plots, to make it easier to see the distribution of the locations. With the exception of one case, all locations are placed within the immediate surrounding of geophone 3. There is no way of knowing if all the events are connected to the block collapse, so the outlier can be an unrelated event. All events are located at the surface, which is expected. The fact that most events are located where the incident happened, indicates that the model is able to locate natural events with some accuracy. Although there are some uncertainty for each case, corresponding to the blue areas in the colour map.

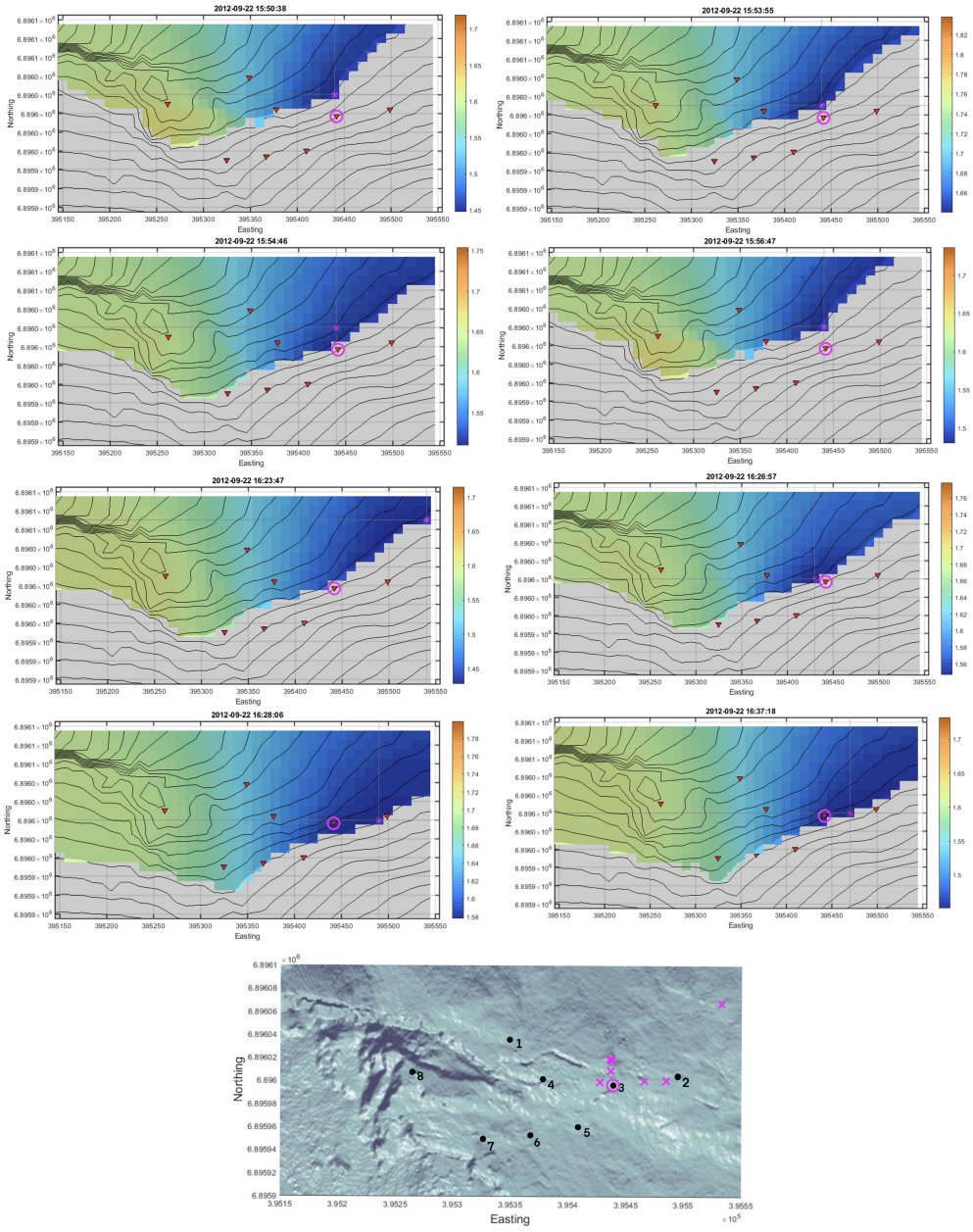

Figure 40: Locations of 8 events which happened around the time of a block collapse from 2012. The locations are marked with pink crosses, and geophone 3 have been marked with a pink circle. The colourbar represent the misfit to the data obtained by the full grid-search location algorithm. The bottom figure combines all locations. The black points show the locations of the geophones.

6 Discussion

The goal for this project was to create a velocity model representing the geologically complex upper part of the unstable Åknes rock slope. The location results when locating the calibration shots from 2006 (with known positions) and some naturally occurring seismic events (with more or less unknown positions), show that the model have been improved for the chosen area. However, the errors in some parts are still relatively large, up to $44m$. In other words, the velocity model is not perfect, and there is still room for improvement.

6.1 First arrivals

When operating with 3D traveltime tables for locations in MStudio, the program makes no distinctions between direct- and head-waves. It only operates with first arrivals, which is why there has been no distinction between the different types of P-waves previously in the project. MStudio could handle both direct- and head-waves when operating with 1D cases. However 1D models are not useful in this project, as we only use homogeneous and 3D models. It is not possible to distinguish between direct- and head-waves in the data set with the naked eye. Even though refracted waves have moved further and therefore often have smaller amplitudes. When the waves were picked, they were simply picked as first arriving P-waves (and in some cases sound-waves). However, it is still important to discuss the wave's assumed ray-paths, as it can be helpful when updating the model. Knowing the ray-paths can suggest which parts of the model are accurate and which parts need improvement. This can be figured out by looking at how the velocity model changes with each step, and how we assume the geology in the area to be.

When working on the 3D heterogeneous velocity model, there are improvements in the results with each new step. The two first versions of the model, are the grid-based and fan-based velocity models (Figures 17, 21). There is a slight improvement in almost all locations obtained with the addition of the fan-based model, compared to the grid-based model alone. They are both based on the velocity map, with straight lines of mean velocities from the shots to the geophones (Figure 15). This means that they only account for

velocity changes in the horizontal plane, and are homogeneous in depth. As the models are based on information only describing the surface of the slope, they follow the assumption that the first arriving waves are direct-waves, which stay close to the surface.

The next step of the model is implementing a velocity increase with depth (Figure 23). Compared to the previous step, most of the location results have been improved. Shots 4, 5 and 6 have been greatly improved, whereas 7 and 9 became less accurate (Table 6). The model has a smooth, gradual velocity increase with depth, and there are no sharp boundary layers. The waves are still affected by the velocities in depth, which means that they must have followed ray-paths deeper than the direct paths. This suggests that some of the first arrivals in the data can be described as diving-waves.

The next step consists of two models containing sliding planes (Figure 25). They are located at depths of $120m$ and $50m$ beneath the surface respectively. The sliding plane at $120m$ depth show some improvements in location results when comparing them to the previous step. The locations of shots 4, 7 and 9 have been improved, while the rest remained unchanged (Table 6). This means that only the waves from three shots have some first arrivals reaching the depths of this sliding plane.

The greatest improvement in the accuracy of the location results happened when the sliding plane at $50m$ depth was implemented. Most of the location results were greatly improved, with the exception of shots 2 and 6, which became slightly less accurate, and shot 10, which remained unaltered (Table 6). This indicates that the waves used in the locations are greatly affected by vertical velocity variations. They must have traveled some portion of their ray-paths along the high velocity layer (the sliding plane). This suggests that the first arriving waves in the data for most of the shots are head-waves.

This study indicates that the sliding plane is located at a depth close to $50m$. It might also be possible with deeper sliding planes or multiple panes beneath the slope. However, this cannot be resolved with the available data set. The shots and geophones are located on the surface of the slope, in a relatively small area. As only a few of the first arrivals

reached the fast velocity layer at $120m$ dept, it is not likely that they would reach any greater depths. In other words, the model can show if there is a high velocity layer at an approximate depth of $50m$, but it cannot prove if there are any other, deeper surfaces. A more detailed data set, covering a larger area, might give the needed information to test if the other suggested sliding plane depths (or other types of surfaces) are present beneath the Åknes rock slope.

The surface of the Åknes rock slope is greatly fractured and deformed, and it will be difficult for waves to travel through the upper parts. It is therefore unlikely that the first arrivals represent direct P-waves, especially for the waves traveling longer distances. On the other hand, the study area is quite small, and the shots and geophones are often located close together. If the first arrivals are head-waves, they would have to move quite far to reach the high velocity layer, before being refracted and heading back to the surface. This would not be realistic for the cases where the shots and geophones are located very close together. If we combine the observations from the model and the assumptions about the geology and distances, we can suggest that direct-, diving- and head-waves might all be present as first arrivals in the data set. Although, if we were to make a conclusion purely based on the results from the model, most of the first arrivals must be head-waves, as implementing the sliding plane at a depth of $50m$ had the largest impact on the results.

6.2 Comparing homogeneous and 3D velocity models

The final 3D velocity model produces superior locations compared to the homogeneous velocity models. However, it is still interesting to examine the locations obtained by the homogeneous velocity models, as these can give an insight into which velocities dominate the study area in general. In other words, it can tell us what the mean velocity should be.

The best homogeneous velocity model based only on P-waves in this project, has a $V_p = 3000m/s$ (Figure 12). It produces much lower RMS errors compared to the models based on lower velocities, and slightly better than the ones based on higher. This suggests

that a P-wave velocity close to $3000m/s$ should be the mean velocity for the study area. Comparing the accuracy of the locations from this homogeneous velocity model with the earliest stage of the 3D model (grid-based), shows that the homogeneous velocity model actually gives better results. However, the velocities used as a base for the grid-based model are from actual measurements at the site. The homogeneous model has an unrealistically high velocity for the upper layers, when taking the knowledge about the geology into account. This indicates that the grid-based velocity models only represent the upper layers of the area, and cannot be used to represent the velocities at depth. To fulfill a mean velocity of $3000m/s$, a high velocity zone must be present in depth. This high velocity area is modelled as the sliding plane at $50m$ depth. In other words, the final 3D velocity model and the best fitting homogeneous velocity model correspond well. This indicates that the velocities chosen for the final 3D velocity model are realistic.

6.3 Limitations

When manually making a 3D velocity model, there is no real limit to how many elements one can add. However, there are other restrictions for the model. The geology of the area is not perfectly understood, and one must rely on assumptions form earlier work.

Another constraint to the model, is the size of the study area, which is limited by the distribution of calibration shots and geophones, and thereby the limited amount of data. Another set of calibration shots, covering a larger area, would increase the size of the study area and the amount of data. This might increase the quality of the model, and also make it possible to run a detailed automated tomography (NORSAR, 2006). Another way to improve the data, would be to expand the geophone network. The knowledge about the geology in depth is also limited by the data. Only a sliding plane at a depth of $50m$ can be determined by the model. It cannot show if there are any other deeper surfaces present.

Time is another limitation, as the process of programming and adding more features to the model is time consuming. A manageable amount of updates and features were added to the velocity model, reflecting the time frame of this project.

6.4 Future work

To further improve this work, we could acquire new and improved data, preferably for a larger area. This would be helpful both for interpreting the geological features like the sliding plane and for improving the velocity model.

For this current model we propose three possible ways of improvement. Firstly, we have presented a way of further testing the models accuracy, by trying to locate known rockfalls in the area. Secondly, we have suggested a possible way to update some of the model's existing features, by smoothing them. Thirdly, we have suggested an additional feature, which can be added to improve the model's overall quality. This feature is a crack running through most of the area.

6.4.1 Further testing of the model's accuracy

In section 5.2 and 5.3 a snow avalanche and a block collapse were located using the model. While the bock collapse was observed, the avalanche damaged a specific geophone. It is safe to assume that the events happened in close proximity to geophone 3 and 2, respectively. These geophones are both located on the eastern side of the model, and are quite close together. Thus, we have only tested the accuracy in a portion of the study area. Similar tests done in proximity to different geophones, would further indicate the model's accuracy.

Such tests could be run using rockfalls. There are several recorded rockfalls, which have destroyed the cables of specific geophones. Because of this, it is possible to guess the approximate locations of the events, as they must have happened close to the geophone they affected. Locating three such rockfalls was tried, but the tests were unsuccessful. The waveforms for rockfalls are difficult to interpret, because they are surface processes. We were not able to pick reliable arrival times for any of the events, and we were not able to get consistent results, using the full grid-search location method. It might be possible to locate these events, using the same velocity model, but a different location method in

future trials. Using the migration-stacking method, which does not require arrival times, but uses the energy of the arriving waves instead (Fischer et al., 2019), might be more suitable. This would be a good way to further test the accuracy of the velocity model, checking how well it represents the velocities in the entire study area.

6.4.2 Smoothing the model

Using a Gaussian filter in MatLab to smooth certain features of the 3D model was planned. However, we ran out of time, making this something which can be done in the future.

The grid-based velocity model, used as a background for the final model, consist of four large cells, with homogeneous velocities (Figure 17). There are no gradual transitions between the different velocity sections. The model might interpret these sharp transitions as layers, which is not what the velocity map or geology suggests. Smoothing the transitions between the velocity zones would make the model more geologically accurate.

The sliding plane is modelled using a file containing every point on the topography of the slope, with 5x5x5m grid-cells. It is modelled as a perfect copy of the topography, moved down to the wanted depth. Even though the sliding plane is suggested to be 50m beneath the surface, this is probably not true for all points. In other words, the sliding plane should not be a perfect copy of the surface. Although it would possibly feature some of the same structures, they would be less distinct. As the actual depth and shape of the plane is unknown, it should be smoothed with a Gaussian filter, softening the sharpest features present in the topography.

The graben structure model covers both the graben and the assumed surrounding low velocity area. It is modelled by an approximately placed ellipse. The edge of the ellipse is sharp. Smoothing this edge might make the model more realistic.

Smoothing the entire model proved pointless, as the features are based on different

amounts of information. Smoothing the entire model at once, could improve it in some areas, while loosing detail in others. For example the grid-based model represents the edges of the study area, where we have the smallest amount information. Smoothing this feature could improve the model, as it would soften the sharp edges between the four quadrants. The fan-based model, on the other hand, represents the middle of the area, where we have the most information. Smoothing this feature with the same filter, would lead to loss of detail.

Even without the use of a filter, the fan-based model might be seen as already smooth. Where the fan-shapes overlap, the mean velocity have been chosen. The center of this model is very smoothed, but the edges could use a bit more work. A way to make this part of the model more realistic could be to apply smoothing to the very edges of the feature, smoothing it with the background.

6.4.3 Modelling the crack

The graben structure in the model is a rough approximation of the structure observed in pictures and maps. A large crack is also present in the study area. However, this crack is not included in our model. It separates geophones 1 and 2 from 3, 4 and 5. The remaining geophones are located on the other side of the graben structure (yellow lines in Figure 3).

The original plan was to model the graben structure and the crack in the same step of the velocity model. It was difficult to figure out where to draw the features based on the available map, without venturing into pure guesswork. Therefore we discarded the feature, and chose to stick with a model of the graben structure alone.

An alternative way to model a representation of the crack, would be to elongate the structure created around the graben. As with the graben structure, we assume that the crack's immediate surroundings consist of a more fractured medium. It could be possible to construct an approximate low velocity area, between the geophones in question, in-

stead of following the crack perfectly. The most important thing is to model it in a way, that will affect the correct ray-paths. This would be possible to do without any more information about the crack.

7 Conclusion

The Åknes rock slope is a geohazardous area in western Norway. A collapse of the slope could result in a destructive tsunami. The highest rate of displacement on the slope is in the upper part. This is also where a permanent seismic network is installed, continuously gathering seismic data. As the upper part of the slope has the highest rate of movement, it is also the area subjected to the most extensional forces. This leads to deformation and fractures. The fractured medium is assumed to have very rapid changes in velocity, making a homogeneous velocity model unsuitable for representing the velocities in the area.

In this project, a heterogeneous, 3D velocity model was constructed. It was based on measurements from the site and assumed geological features. This new velocity model of the area, produced improved results when locating surface shots with known locations. It was also used to locate naturally occurring events, placing them in expected areas, which suggests that the model is a good representation for the varying velocities in the area.

The final 3D velocity model is useful when locating seismic events at Åknes. In the future, this model might be improved by adding more features. It will be used by NORSAR in daily processing, and in their ongoing work towards improving the real-time warning system for the unstable Åknes rock slope.

References

Blikra, L., Longva, O., Braathen, A., Anda, E., Dehls, J., and Stalsberg, K. (2006). Rock slope failures in norwegian fjord areas: examples, spatial distribution and temporal pattern. In *Landslides from massive rock slope failure*, pages 475–496. Springer.

Blikra, L. H., Kristensen, L., and Lovisolo, M. (2013). Subsurface monitoring of large rockslides in norway: a key requirement for early warning. *Ital. J. Eng. Geol. Environ*, 6:307–314.

Boadu, F. K. (1997). Fractured rock mass characterization parameters and seismic properties: analytical studies. *Journal of Applied Geophysics*, 37(1):1–19.

Braathen, A., Blikra, L. H., Berg, S. S., and Karlsen, F. (2004). Rock-slope failures in norway; type, geometry, deformation mechanisms and stability. *Norwegian Journal of Geology/Norsk Geologisk Forening*, 84(1).

Fischer, T., Kühn, D., and Roth, M. (2019). Microseismic events on the åknes rockslide in norway located by a back-projection approach. *Journal of Seismology*, pages 1–20.

Harbitz, C., Glimsdal, S., Løvholt, F., Kveldsvik, V., Pedersen, G., and Jensen, A. (2014). Rockslide tsunamis in complex fjords: from an unstable rock slope at åkerneset to tsunami risk in western norway. *Coastal engineering*, 88:101–122.

Kveldsvik, V. (2008). Static and dynamic stability analyses of the 800m high åknes rock slope, western norway.

Langet, N. (2018). Norsar internal report: Automatic processing of the åknes surface data.

Nordvik, T., Grøneng, G., Ganerød, G. V., Nilsen, B., Harding, C., and Blikra, L. H. (2009). Geovisualization, geometric modelling and volume estimation of the åknes rockslide, western norway. *Bulletin of engineering geology and the environment*, 68(2):245–256.

NORSAR (2006). Norsar internal report: Active seismic experiment at åknes.

Raanes, P. N. (2011). patricknraanes/fm: Version 1.0.

Retailleau, L., Shapiro, N., Guilbert, J., Campillo, M., and Roux, P. (2015). Detecting and locating seismic events with using usarray as a large antenna. *Advances in Geosciences*, 40(40):27–27.

Roth, M., Dietrich, M., Blikra, L. H., and Lecomte, I. (2006). Seismic monitoring of the unstable rock slope site at åknes, norway. In *19th EEGS Symposium on the Application of Geophysics to Engineering and Environmental Problems*, pages cp–181. European Association of Geoscientists & Engineers.

Wuestefeld, A., Greve, S. M., Näsholm, S. P., and Oye, V. (2018). Benchmarking earthquake location algorithms: A synthetic comparison. *Geophysics*, 83(4):KS35–KS47.